water

MDPI

Article

Flood Vulnerability Study of a Roadway Bridge Subjected to Hydrodynamic Actions, Local Scour and Wood Debris Accumulation

Mirko Kosič, Andrej Anžlin and Valentina Bau' *

Slovenian National Building and Civil Engineering Institute (ZAG), Dimičeva ulica 12, 1000 Ljubljana, Slovenia
* Correspondence: valentina.bau@zag.si

Abstract: The increased occurrence and intensity of flooding events have represented a real threat to bridge reliability and end-user safety. As flood vulnerability assessment is a valuable tool for enhancing the resilience of bridges to climate change, it is of interest to push the development of such methods. To this end, a computationally efficient methodology to assess the flood vulnerability of a bridge was developed and implemented in a case study. A particular focus was devoted to modelling wood debris loads on the bridge pier, for which two different approaches were implemented. The first is a standards-based approach, whereas the second is based on up-to-date research data. The results indicate that the second approach is less conservative as it leads up to a 40% higher exceedance probability for the considered limit states. The interaction between wood debris loads and local scour was also examined and proved to have a relevant impact on the vulnerability of the bridge. These results highlight the shortcomings of the existing standards in providing accurate results. It is perceived that not only will the new quantitative tool be valuable in ensuring optimal bridge design, but it will also be beneficial for assessing bridge risk mitigation measures.

Keywords: flooding; vulnerability; wood debris; local scour; hydrodynamic load; stochastic approach; bridges

Citation: Kosič, M.; Anžlin, A.; Bau', V. Flood Vulnerability Study of a Roadway Bridge Subjected to Hydrodynamic Actions, Local Scour and Wood Debris Accumulation. *Water* **2023**, *15*, 129. https://doi.org/10.3390/w15010129

Academic Editors: José González-Cao, D. Fernández-Nóvoa and Orlando Garcia Feal

Received: 2 December 2022
Revised: 20 December 2022
Accepted: 22 December 2022
Published: 29 December 2022

1. Introduction

Bridges have a fundamental role in transportation infrastructure and the overall world economy; as such, their targeted performance must be met. Complying with the requirements for modern bridge design requires accurate modelling and a careful analysis of the vulnerability to natural hazards. Local scour and other hydraulic-related processes (e.g., channel migration, flood-associated loads, and wood debris accumulation) have been proven to be the main reasons for bridge collapse [1], thus affecting the functionality of the transport system. Evidence of such a pivotal danger is the scientific literature, which has reported several failures of infrastructures triggered by flooding events in the USA, the United Kingdom, and Europe [2–6]. In this last decade, scientists and practitioners have put considerable effort into focusing on the vulnerability of riverine bridges to natural hazards, particularly flooding and local scouring events [7].

The structural integrity of bridges that cross rivers can be compromised by hydrodynamic forces as well as by the loading effect caused by the accumulation of floating wood debris at the piers. Most commonly, the type of debris that endangers bridge safety consists of waterborne debris (e.g., tree trunks and limbs) that are transported by the water current during flooding events [8]. The presence of debris jams at the piers of bridges may cause an increase in the upstream water levels (*afflux*) and a backwater effect, thus posing an additional flood hazard for the nearby areas [9]. Wood debris, once stranded at the piers, can also lead to an increase in the hydrodynamic actions and trigger an exacerbation of the local scour [10]. Local scour is an equally threatening process that can lead to uncovering the piers' foundations and reducing their lateral stiffness and load-bearing capacity [11].

Local scour at bridges results from the removal of sediment from around the base of the pier caused by the onset of horseshoe vortices [12]. The action exerted by local scour has been responsible for 60% of bridge failures in the United States, according to [13]. Despite a variety of failure modes associated with local scour, vertical and lateral modes were most frequently observed [14]. Therefore, it is evident that flood-induced hydrodynamic and debris impact can undermine the structural safety of bridges and lead to severe structural damage and consequent economic losses [15].

In order to assess the vulnerability of bridges to floods and develop resilient countermeasure strategies, the implementation of fragility curves represents a reliable and consolidated methodology [16]. Unlike deterministic approaches, vulnerability analysis consists of computing the conditional probability of exceedance of a defined damage state for a considered hazard or a combination of them. While the vulnerability of bridges to seismic performance has been widely investigated [17–21], little is known about how flooding events and related processes can simultaneously affect the structural vulnerability of a bridge. Moreover, although the flood-related risk was included in seismic vulnerability analysis, its contributions were not considered the main cause of bridge failure [22,23]. Nevertheless, due to the incumbency of changes in global climate, recent studies have started to implement a more accurate vulnerability analysis of bridges against floods. For instance, the authors of [24] carried out a flood vulnerability analysis by taking into account the simultaneous contribution of bridge scour, structural deterioration of the steel reinforcements and piles, and the increased water pressure due to debris accumulation around bridge piers. Another approach was presented by [25], who included the geotechnical uncertainties provided by the foundation design in the vulnerability analysis. Additionally, the authors of [26] presented a holistic approach where the fragility curves were implemented examining different combinations of scouring conditions and earthquake loadings for a reinforced concrete bridge with shallow foundations. Another efficient framework has been introduced by [27], who identified the possible modes to bridge failure caused by scour-related processes. An interesting perspective is also offered by [28], who provides a performance-based engineering framework on a flood fragility analysis of a bridge subjected to various loading scenarios and local scour. Fragility curves were also employed to illustrate the exceedance probability of the limit states of a masonry bridge exposed to scour-induced support rotation [29]. In spite of the lack of a classic fragility analysis approach, the authors of [30] offer a comprehensive and innovative analysis of local scour. Using artificial intelligence techniques, the authors implement a probabilistic methodology that can predict scour depths created by regular waves on groups of piles. It is also discussed that probabilistic approaches should be able to incorporate uncertainties for the most critical parameters that influence local scour depths (e.g., pile diameter, average flow velocity) [31].

Driven by these emerging research perspectives, the presented framework refers to a vulnerability analysis methodology that aims at using a probabilistic approach to grasp some of the uncertain variables that affect bridge resilience to floods. Particular focus is placed on the procedure for modelling wood debris accumulation on the bridge piers. The vulnerability analysis of this study is implemented for both the serviceability and ultimate limit state to provide an overall view of the structure's performance. The variability of material and geotechnical properties, hydrodynamic loading, wood debris size accumulation, and scour magnitude is taken into account to illustrate different scenarios through the analytical implementation of vulnerability surfaces and two failure modes. The process of a random sampling of the variables is performed with a very efficient stratified sampling approach (i.e., Latin Hypercube Sampling (LHS)), thus abandoning the typical Monte Carlo simulation.

The strength and stiffness of the construction materials (e.g., concrete and reinforcing steel) are some of the major sources of uncertainties in civil engineering structures. Their assigned values are critical determinants of the behavior of a structure [32]. Thorough studies have been undertaken to assess the statistical parameters and models of materials

properties [33,34], thus providing solid support when considering such uncertainties in vulnerability analysis. Similarly, the natural variability of soil properties and especially the influence of soil spatial variability on structural performance have also been widely investigated [35,36]. The same cannot be said when considering the uncertainties provided by the actions of flood and wood debris loading and local scouring. The gap in information and criteria to incorporate flood-related processes into the vulnerability analysis of bridges, as opposed to earthquakes, may be due to the difficulties related to monitoring such processes. The complexity of hydraulic data, the high cost of monitoring techniques, and the stochasticity inherent in flood-related processes may discourage researchers and practitioners from exploring such crucial conditions for bridge vulnerability evaluation [37].

This work aims to implement the aforementioned methodology and create a reliability analysis framework to investigate flood vulnerability through a real-bridge case study. The originality of this paper stands in offering an analysis framework that considers the addition of both hydraulics and geotechnical model uncertainties to the ones that are commonly established in the vulnerability analysis of bridges (e.g., material uncertainties). The novelty of this paper also relies upon the way the vulnerability analysis is addressed. The largest part of the existing studies on bridge vulnerability analysis has often modelled the hydrodynamic and wood debris loads by referring to government guidelines or bridge design specifications (e.g., AASHTO LRFD Bridge Design Specification [25]). However, such references are rather simplistic and differ widely due to a lack of consistency in cross-countries methodology comparisons [13,38]. Furthermore, the use of regulations and standard specifications can lead to an inherent conservatism that is not beneficial for vulnerability analysis since it overestimates the probability of reaching the considered damage limit state analysis. For this reason, the goal of this study is to utilize the latest research outputs to provide a different perspective and a source of comparison to the most relevant existing guidelines.

2. Materials and Methods

2.1. Material Properties and Input Data

2.1.1. Geometry and Materials

The case study is a historic roadway riverine steel bridge located in central Croatia. The bridge has two main spans, a total length of approximately 97 m and a total width of 12.4 m. It supports two traffic lanes and a pedestrian zone. Information on the geometry and materials of the bridge was retrieved from relevant as-built construction information, a recent retrofitting project, and a drone survey. The overview and the geometrical characteristics of the bridge are illustrated in Figures 1 and 2, respectively.

The two main girders have riveted I-shape cross-sections with flanges whose thickness variation follows the bending moment line. The main girders are joined together every 4.05 m by riveted transverse beams that are connected with seven I-shaped stringers that, in turn, support the reinforced concrete (RC) slab of the deck (Figure 1c).

At the abutments, the bridge is supported by longitudinal roller bearings with a diameter of 20 cm (Figure 1d). The transverse displacement of each bearing is restrained with shear keys of size 0.03 × 0.06 m. At the pier, the translation of the deck is restrained in all directions by the presence of shear pins with a diameter of 0.05 m. The pier and the abutments are made of reinforced concrete and are covered with 15 cm stone cladding. The middle pier has a rectangular section with rounded ends (see Figure 2b) and is founded on two large well foundations of 6.5 m diameter (D). Due to the unavailability of as-built construction plans, the depth of each foundation is assumed to be equal to that used in the pre-existing bridge from 1889 (L = 5.8 m), for which partial historic construction plans were obtained.

Figure 1. Overview of the case-study bridge: (**a**) side view, (**b**) detailed view of the middle pier and well foundations, (**c**) view below the bridge deck, and (**d**) detailed view of the roller bearing at the abutment.

The mechanical characteristics of the superstructure were gained through the destructive testing performed within the retrofitting project. The steel grade used for the superstructure is estimated to be equivalent to S235 according to EN-1993 [39], whereas the grade of concrete of the deck is assigned a grade of C25/30 according to EN-1992-1 [40]. In the absence of the material characteristics used for the bridge piers and foundations, the grade of the concrete is assumed to be the same as for the bridge deck (C25/30).

2.1.2. Geotechnical Data

The input data for the modelling of the soil–structure interaction (SSI) at the bridge's central foundation were obtained from a Cone Penetration Test investigation (CPT) and a borehole performed near the bridge's abutment. The soil profile consists of a top 6 m of clay layer with an underlying medium-dense sand layer. Investigations conducted directly near the foundation of the central pier are not available. However, geophysical profiling indicated that the stratigraphy occurring near the bridge's abutment also occurs near the foundation. Hence, the foundation is assumed to be located in the medium-dense sand layer. The estimated soil characteristics for modelling the soil–structure interaction at the central pier are summarized in Table 1.

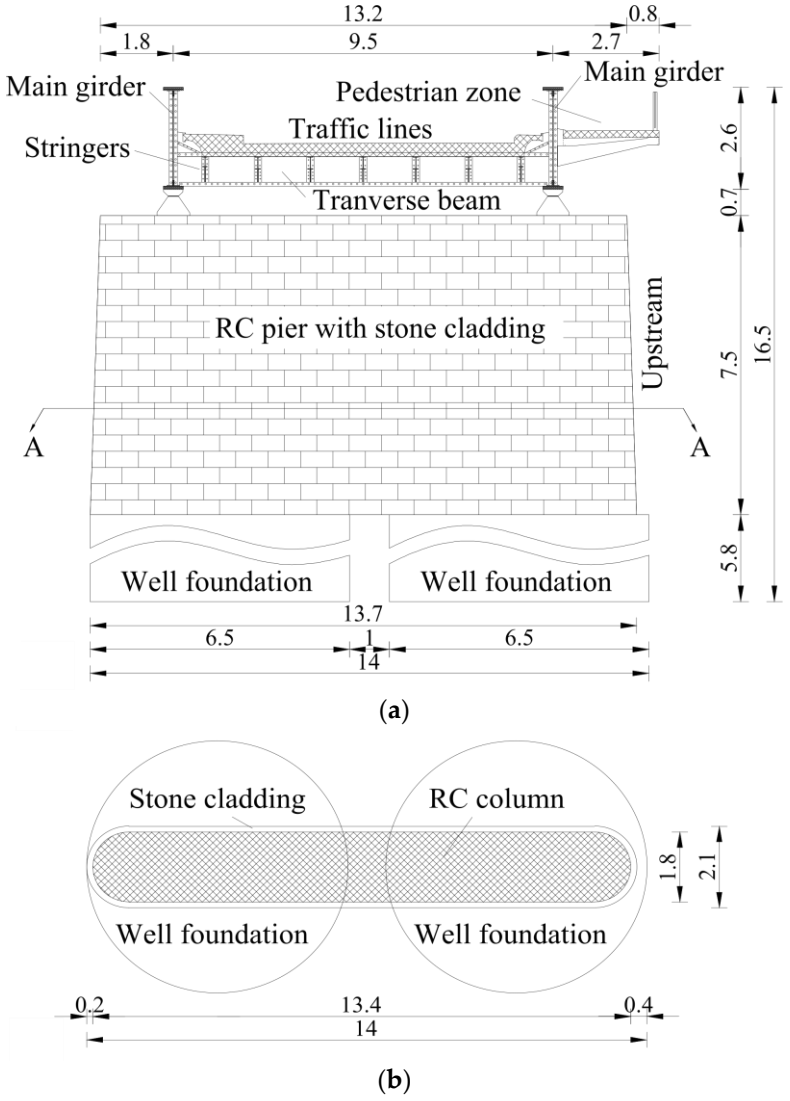

Figure 2. (**a**) Cross-section of the case-study bridge; (**b**) cross-section A-A at the base of the pier.

Table 1. Soil characteristics used for modelling the soil–structure interaction at the central pier of the bridge.

Parameters	Value
Effective shear angle (φ')	40°
Effective cohesion (c')	0 kPa
Soil unit weight (γ)	19.8 kN/m^3
Poisson's ratio (ν)	0.30
Elastic modulus (E)	50 Mpa
Shear modulus (G)	19 Mpa
Equivalent SPT blows (N_{60})	19

2.1.3. Hydraulic Data

The hydraulic data was retrieved based on existing numerical simulation results. In particular, the data from the simulations refer to the maximum daily values computed for extreme past flooding events that occurred in 2014 and 2015, respectively. In Figure 3a,b, the relationships between the water height (H) and water discharge (Q), and between the water height (H) and flow velocities (v), respectively, illustrate the complex hydraulic conditions encountered at the location. The data dispersion suggest that the hydraulic conditions are

strongly affected by the variable backwater effect of the tributary river located downstream from the bridge.

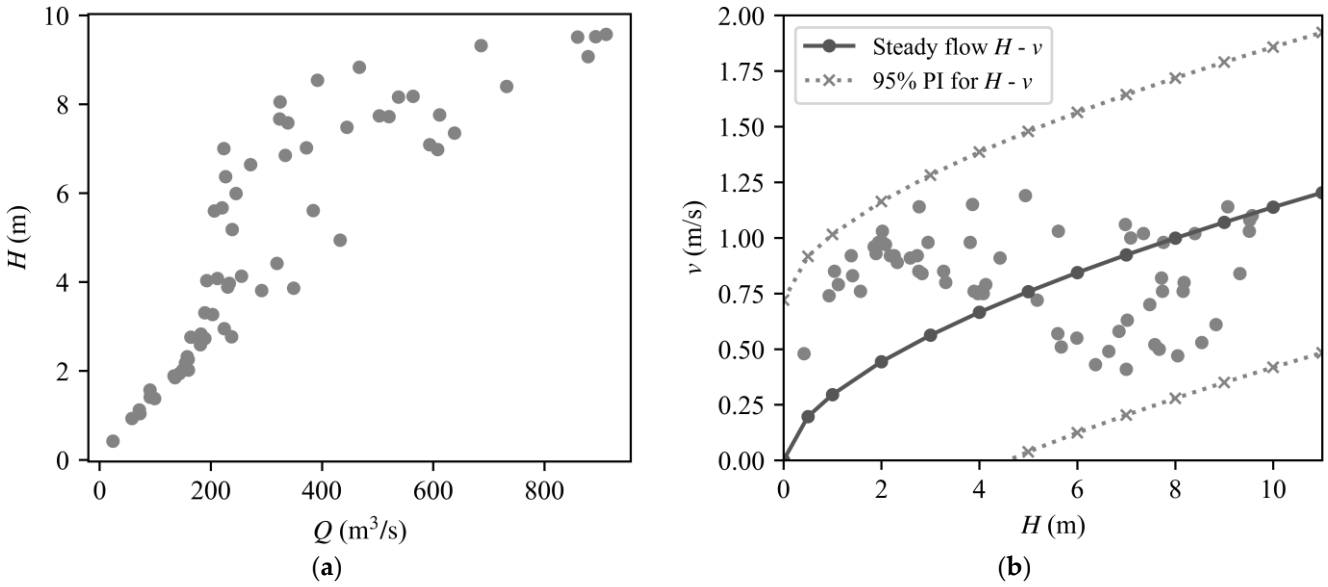

Figure 3. Results obtained from the numerical simulations of two flooding events. (**a**) Relation between water height (H) and discharge (Q); (**b**) relation between water velocity (v) and water height (H). The steady flow relationship and the 95% prediction interval curves are also represented.

Furthermore, the limited amount of data makes it hard to detect a particular hysteretic pattern or any particular trend in the data. Given the circumstances, the vulnerability analysis cannot rely on a unique $H - v$ relationship and is therefore implemented for unsteady flow conditions (i.e., with consideration of both flow velocities and water heights as input parameters).

The vulnerability assessment is performed within the bounds marked by the 95% prediction intervals (PI) obtained from the regression of the data with the steady-flow Manning's equation [41]. Knowing the intervals within which new observations are likely to fall makes it possible to explore flooding scenarios that are also more severe than the ones registered in 2014 and 2015, providing an idea of the limit states that the structure may encounter if certain water heights and flow velocities were reached.

Note that the computations are carried out considering a limit for the water heights of 10.8 m, which corresponds to the full submergence of the deck of the bridge, and a minimum flow velocity of 0.1 m/s, as velocities below this value, are irrelevant for the purpose of this study.

2.2. Methodology and Modelling Approach

2.2.1. Overview

The complete flowchart of the proposed framework is presented in Figure 4. As can be seen in the flowchart, both deterministic and stochastic modelling approaches are used.

The vulnerability analysis begins with determining the external forces acting on the bridge (e.g., hydrodynamic forces, gravity forces, and loads resulting from wood debris accumulation) that, along with other data inputs (geotechnical data, bridge geometry, and local scour assessment), are necessary to implement the structural finite-element modelling and the soil–structure interaction. These parameters combined represent the deterministic model of the bridge, which specifies the computation of the structural behavior of the bridge based on a particular set of input information. Details regarding the structural finite-element, the soil–structure interaction, load and local scour modelling are presented in Sections 2.2.2–2.2.5, respectively.

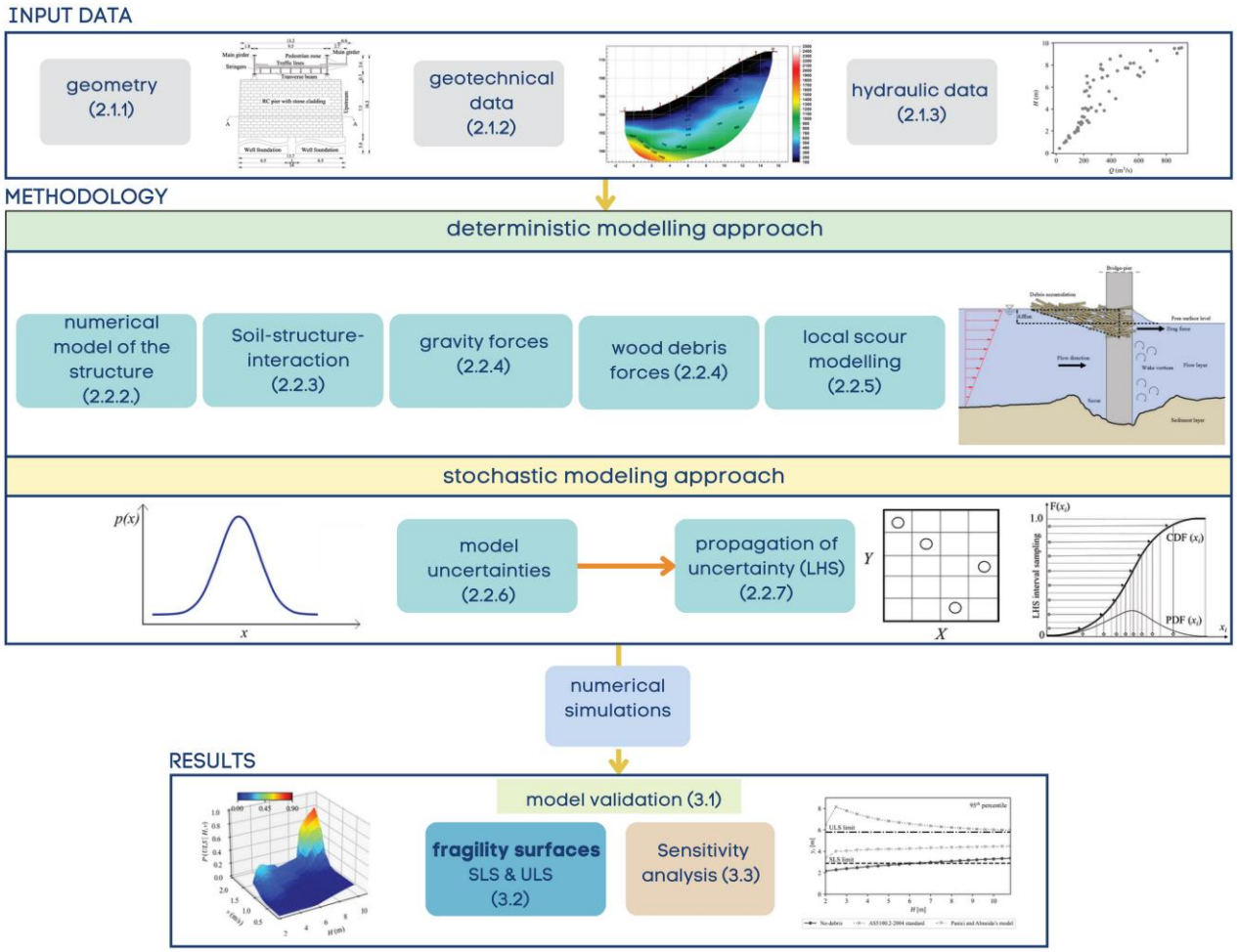

Figure 4. Flowchart illustrating the procedure that is implemented for the flood vulnerability analysis of the bridge.

The deterministic model is converted into stochastic in the second step. In this way, it becomes possible to include in the model the variability of the input parameters that defines the probabilistic distribution of the loading actions and resistance of the bridge. In this study, it is assumed that the probabilistic distribution of the limit states of the bridge is related to the variability of the material characteristics (concrete strength, steel yield strength and elastic modulus), geotechnical properties of the soil (soil shear modulus, effective shear angle, and unit weight), hydrodynamic forces, local scour depths, and size of wood debris accumulation. The details regarding the considered uncertainty parameters are provided in Section 2.2.6.

As part of the next step, the propagation of the uncertainty of the model's inputs is implemented through the use of Latin Hypercube Sampling (LHS), which is described in Section 2.2.7. The advantage of this method is that it reduces the number of simulations significantly, which makes it more computationally efficient than Monte Carlo approach.

After the model uncertainties are propagated, it is possible to generate the fragility surfaces of the bridge. The fragility surfaces indicate the probability of reaching or exceeding a designated limit state (LS) for a given level of flood intensity (Intensity Measure, IM). Generally, the exceedance probability of a designated LS is represented by the so-called fragility curve. However, in this study, due to the lack of a univocal $H - v$ relationship, the IM is defined based on both parameters (i.e., H and v). Therefore, the probability of exceeding a designated LS is expressed as $P(LS|\, H, v)$ and is represented by a fragility surface.

In this study, the serviceability limit state (SLS) as well as the ultimate limit state (ULS) are analyzed. The first is assumed to be related to the operability of the bridge during

flooding, whereas the latter is related to the capacity of the bridge to withstand flooding events without collapsing.

2.2.2. Structural Finite-Element Modelling

A 3D numerical model of the bridge is generated in the OpenSeesPy Library [42], an open-source Python3 interpreter for OpenSees [43]. The modelling approach relies on linear elastic beam elements and zeros length-elements soil springs for modelling the soil–structure interaction. A user-defined toolbox is developed in the Python environment in order to carry out a fully parameterized analysis for bridges subjected to hydrodynamic and wood debris loads in combination with the scouring action on the piers.

A schematic representation of the model is presented in Figure 5. Each bridge member is modelled with linear elastic Timoshenko beam-column elements. The load transfer between individual beam elements is achieved by the definition of fictitious infinitely stiff and weightless elements (stiff elements), which are used to connect the centroid lines of the elements. A more precise distribution of the forces in the bearing at the abutments and the middle pier is gained by positioning the bearing at their actual location in plan and elevation using rigid elements (see Figure 5). The deck of the bridge is modelled with an equivalent beam element. The boundary conditions at the abutments simulate the roller bearings' behavior (i.e., free translation in the longitudinal direction and free rotations). The bearings at the pier are modelled as pinned.

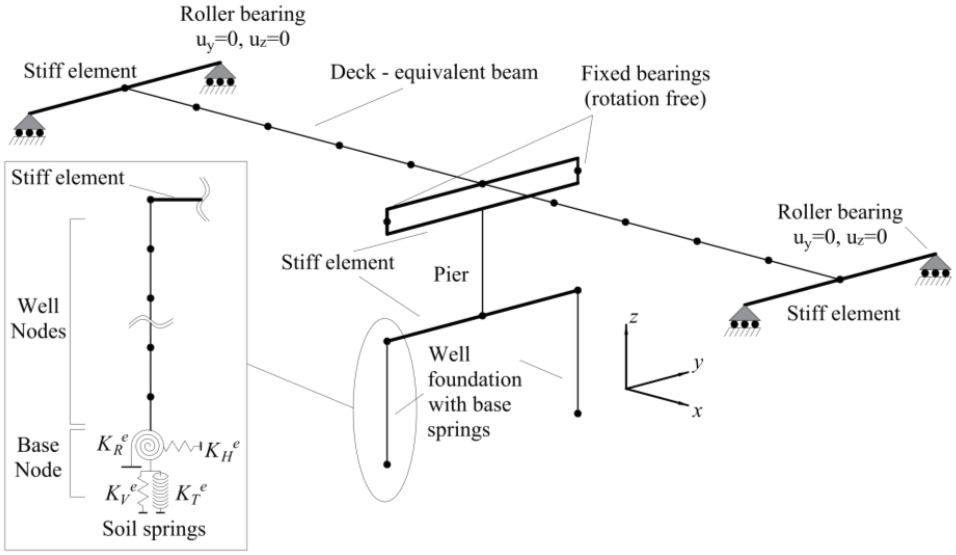

Figure 5. Scheme of the numerical model of the case-study bridge.

2.2.3. Soil–Structure Interaction Modelling

The soil–structure interaction at the well foundations is modelled with a lumped-spring approach. Due to the small ratio between the depths and their diameters ($\frac{L}{D} = \frac{5.8}{6.5} = 0.90$), the wells are modelled as embedded shallow foundations. In such a case, the SSI is modelled with six mutually independent springs located at the base of each well. Figure 5 shows only a scheme of springs with a unique definition, i.e., two horizontal and two rotational springs have the same characteristics in two different directions. The springs are aggregated into a single zero-length element, which connects the base of the well with a fully restrained node. The static stiffness of the foundation springs is calculated following the solution found for embedded cylindrical foundations by Pais and Kausel [44]. The solution considers soil as a linear-elastic material and the foundation as a rigid body, with the presence of a non-slip interface between the foundation and the soil. The influence of the foundation embedment is taken into account through amplification factors, which are applied to the solution obtained for surface foundations. The vertical

(K_V^e), horizontal (K_H^e), rocking (K_R^e), and torsional (K_T^e), stiffness of the (embedded) well foundation are computed as follows:

$$K_V^e = K_V^0 \left(1 + 0.54\, D_E/R_f\right) = \frac{4\, G\, R_f}{1-\nu} \left(1 + 0.54\, D_E/R_f\right) \quad (1)$$

$$K_H^e = K_H^0 \left(1 + D_E/R_f\right) = \frac{8\, G\, R_f}{2-\nu} \left(1 + D_E/R_f\right) \quad (2)$$

$$K_R^e = K_R^0 \left(1 + D_E/R_f\right) = \frac{8\, G\, {R_f}^3}{3\,(1-\nu)} \left(1 + 2.3\, D_E/R_f + 0.58 \left(D_E/R_f\right)^3\right) \quad (3)$$

$$K_T^e = K_T^0 \left(1 + D_E/R_f\right) = \frac{16\, G\, {R_f}^3}{3} \left(1 + 2.67\, D_E/R_f\right) \quad (4)$$

where R_f is the radius, D_E is the embedment depth of the foundation, and G and ν are the shear modulus and Poisson's ratio of the soil, respectively. The superscript e denotes the stiffness of the embedded foundation, whereas the stiffness of the surface foundation is denoted by the 0 superscript.

2.2.4. Loads Modelling

Loads on the structure come from gravity (self-weight and permanent loads), hydrodynamic forces (drag F_d and lift forces F_l), buoyancy forces, and wood debris accumulation. In the numerical model, each load is computed per unit length and is applied uniformly.

The loads are combined to produce the maximum possible overturning action on the bridge, which occurs when horizontal hydrodynamic and wood debris loads are combined with an uplift action on the deck. In such a case, the hydrodynamic uplift of the deck is combined with the buoyancy. For this reason, the simultaneous presence of traffic loads is not considered, as this would result in a stabilizing action on the bridge.

The hydrodynamic loads are only applied to the areas of the bridge that are not affected by debris loads to avoid the duplication of hydrodynamic actions.

Hydrodynamic Forces

The hydrodynamic forces are computed according to the Australian standard AS5100.2-2004 [45]. Due to its comprehensive approach, the Australian standard is chosen over the ASSHTO standard, since it provides additional guidelines for quantifying the hydrodynamic loading on the bridge's deck. The drag force in the direction of the flow (in kN) is defined as follows:

$$F_d = 0.5\, C_d\, v^2\, A_d \quad (5)$$

where C_d is the drag coefficient, v is the average water velocity and A_d is projected wetted area in the direction of the flow. According to the Australian standard, for piers with semi-circular nosing such as the case study bridge's pier, the coefficient C_d equals 0.7. For the deck of the bridge, the coefficient C_d is instead computed as a function of the relative submergence of the deck (S_r) and proximity ratio (P_r), which are, respectively, defined as:

$$S_r = \frac{d_{wgs}}{d_{sp}} \text{ and } P_r = \frac{y_{gs}}{d_{ss}} \quad (6)$$

where d_{wgs} is the distance from the girder soffit to flood water surface, d_{sp} is the wetted depth of the deck (including any railing and parapets), y_{gs} is the average vertical distance from the girder soffit to the riverbed, and d_{ss} is the wetted depth of the solid superstructure (excluding railing but including parapets).

The lift force on the bridge pier and deck (in kN) is computed with the following equation:

$$F_l = 0.5\, C_l\, v^2\, A_l \quad (7)$$

where C_l is the lift coefficient, and A_l is the wetted area perpendicular to the flow.

In this study, the lift force is only computed in relation to the deck in the cases when it is submerged. The lift force on the pier is neglected as the pier is oriented in the direction of the flow. The coefficient C_l for the bridge deck depends on its relative submergence (S_r).

As indicated in the literature ([24,25,46,47]), the distribution of the hydrodynamic forces over the water height can be well approximated by a triangular shape. The triangular distribution of the forces yields a lower safety margin than a uniform distribution because it results in a larger overturning moment above the base of the foundation.

The buoyancy force is computed as the weight of the displaced water and is applied concurrently with the upward lift force on the bridge's deck. The magnitude of the buoyancy force varies according to the level of submergence of the deck. The buoyancy force increases with the level of submergence of the deck and reaches its maximum value when the deck is fully submerged.

Wood Debris Forces

Wood debris load is modelled with two different approaches to benchmark its impact on the flood vulnerability of the bridge. The first approach is based on the guidelines provided by the Australian standard (AS5100.2-2004), whereas the second one refers to a recent model drawn from the scientific literature that is herein introduced as Panici and Almeida's model [48]. For the sake of simplicity, henceforth, the word wood debris will be simply referred to as debris.

As per Australian standard, the debris mat has a rectangular shape, with height and width indicated. In the absence of more accurate estimates, the minimum height of the wood debris mat (H_d) is set to be between 1.2 and 3 m. Depending on whether the debris accumulation is acting on the bridge deck or the pier, the width of the debris mat changes (W_d). In the case of debris acting on the bridge's piers, the width of the debris mat is assumed to be the smallest value between one-half of the sum of the adjacent spans' length (S_L) and 20 m. In the case of debris acting on the bridge deck, the projected width of the debris mat is equal to the projected length of the deck (D_L). For the purpose of this study, the height of the debris is set at 2.1 m, which is the mean value of the suggested range.

It should be noted that AS5100.2-2004 [45] does not provide the length of the debris mat in the flow direction (L_d).

For the second approach [48], the debris modelling has been implemented by referring to the regression curves obtained when experimenting on the jam formation of debris with no uniform length on bridges with a single pier. The debris width, height and length are calculated considering the following relationships:

$$W_d = \left(0.77 + 0.94\, e^{-6.14\ Fr_L}\right) L_L \tag{8}$$

$$H_d = \left(0.39 - 0.46\, e^{-5.77\ Fr_L}\right) L_L \tag{9}$$

$$L_d = \left(0.25 + 1.18\, e^{-15.04\ Fr_L}\right) L_L \tag{10}$$

for $0.10 < Fr_L < 0.40$.

W_d, H_d, and L_d are the width, height, and length of the debris accumulations, respectively (see Figure 6). $Fr_L = v/\sqrt{gL_L}$ is the debris Froude number, g is the gravitational acceleration, and L_L is the so-called key log length. The key log is the key element that triggers the accumulation of debris on the pier of the bridge and is represented by the longest wood debris that can be encountered in the upstream reach of the river [48]. In contrast to the recommendation of the Australian standard, the shape of the debris mat is not rectangular but resembles a half-cone pointing downward (see Figure 6). In addition, the size of the debris accumulation depends on the flow velocity.

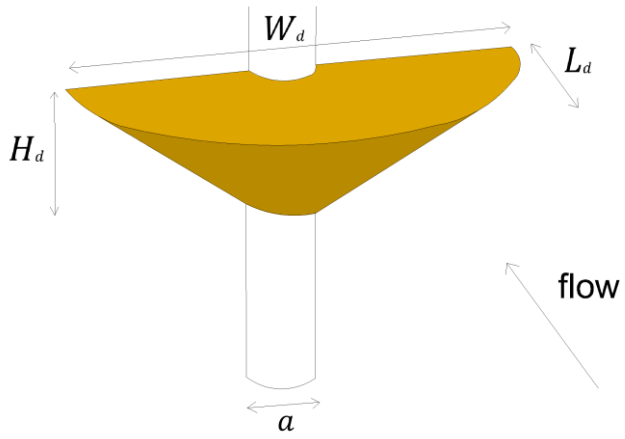

Figure 6. Idealized sketch of a debris accumulation at the bridge pier according to Panici and Almeida's model [48]. Figure adapted from the same source [48].

Equations (8)–(11) can only be solved after inputting the values of flow velocities and assigning an appropriate key log length L_L. The assessment of L_L is not trivial, as this would require persistent monitoring campaigns (i.e., aerial imagery) of the river and riparian areas. As data on wood debris dynamics are missing, L_L has to be selected from one of the few datasets available in the literature. In particular, L_L is selected as the 95% percentile of the probability density function representing the datasets of debris lengths observed in the South River (Virginia, United States) by [49]. The probability density function that best fits the data is a log-normal distribution, which was also used by [48] to reproduce the length distribution of the logs in the experiments. It is interesting to see that the dataset published by [49] is somehow representative of the range of wood length frequencies found in many rivers throughout the world (e.g., Chile, North Germany, Italy, and New Zealand) [50]. Based on the above observation, the employed dataset is deemed to be a good representative of the length of wood debris in general and can hence be used also for the subject river. The value found for L_L is 16 m, which complies well with the highest range of heights of willow trees recorded in the basin to which the river belongs [51].

For the sake of clarity, Table 2 is introduced to outline the comparison between the two debris modelling approaches. It is clear that, while for the first approach the debris accumulation size is constant regardless of the hydraulic conditions, for the second approach, W_d, L_d, H_d vary with bulk flow characteristics and the length of the key log. Hence, it is clear that the AS5100.2-2004 standard provides a more rigid and simplistic approach compared to what is proposed by [48].

Table 2. Properties assigned to wood debris accumulation according to the two modelling approaches.

	Wood Debris Accumulation Properties			
	shape	H_d	W_d	L_d
AS5100.2-2004	rectangular	1.2–3 m	Pier: $W_d = min\begin{cases} 20\ m \\ \frac{1}{2}\sum S_L \end{cases}$ Deck : $W_d = D_L$	not specified
Panici and Almeida's model [48]	half conical	$f(v, g,\ H, L_L)$	$f(v, g,\ H, L_L)$	$f(v, g, H, L_L)$

The magnitude of the drag force exerted by the debris jam is primarily a function of the geometry of the debris accumulation and can be assessed through the empirical drag equation (see Equation (5)). The drag force acting on the area of the pier underneath the debris accumulation is also considered.

2.2.5. Local Scour Modelling

The depth of the local scour is computed according to the HEC-18 equation [52]:

$$y_s = \left[2.0\ K_1\ K_2\ K_3 \left(\frac{H}{a}\right)^{0.35} Fr^{0.43}\right] a \tag{11}$$

where K_1, K_2, and K_3 are the correction factors for the pier nose shape, the angle of attack of flow (θ), and riverbed conditions, respectively. a is the pier width, whereas Fr is the Froude number and is defined as:

$$Fr = \frac{v}{(g\ H)^{1/2}} \tag{12}$$

where v is the mean flow velocity upstream of the pier, g is the acceleration of gravity, and H is the water height upstream of the pier. For round-nose piers with an angle of attack of flow (θ) equal to zero, the coefficients K_1 and K_2 both amount to 1.0. For clear-water scour, K_3 is equal to 1.1.

There is also value in considering the impact of debris on the local scour. The effect of debris on the local scour of the pier is computed following the approach proposed by Lagasse et al. [53]. The approach relies on the quantification of the equivalent pier width (a_d^*), which is then used in Equation (11) instead of a to quantify the scour depth when considering a debris jam. The equivalent pier width is defined as:

$$a_d^* = \frac{K_{d1}(H_d\ W_d)\ (L_d/H)^{K_{d2}} + (H - K_{d1}\ H_d)\ a}{H} \quad \text{for} \quad L_d/H > 1.0 \tag{13}$$

$$a_d^* = \frac{K_{d1}(H_d\ W_d) + (H - K_{d1}\ H_d)\ a}{H} \quad \text{for} \quad L_d/H \leq 1.0 \tag{14}$$

where K_{d1} and K_{d2} are factors depending on the shape of the debris raft ($K_{d1} = 0.79$ and $K_{d2} = -0.79$ for rectangular debris raft; $K_{d1} = 0.21$ and $K_{d2} = -0.17$ for triangular debris raft), and H is the depth of the approaching flow. Due to the lack of recommendations in the Australian standard [45], L_d is set to be equal to H. This condition, according to Equations (13) and (14) [53], allows the reproduction of the largest amplification of the scour for each $H - v$ considered.

Effect of Local Scour on SSI and Flood Loading

The action of the local scour on SSI and flood loading is modelled by reducing the foundation embedded length (D_E) in Equations (1)–(4). Reducing D_E leads to a lower vertical, horizontal, rotational, and torsional stiffness of the foundation, which, in turn, results in the higher flexibility of the pier of the bridge. As a result, a redistribution of the flooding action between the central pier and the embankments and an additional settlement of the central pier is ascertained.

In addition to the above-mentioned consequence, local scour may cause the exposure of the foundation, thus leading to additional hydrodynamic loading. This effect is included by assigning additional drag forces on the part of the foundation that is exposed due to scour.

2.2.6. Parameters' Uncertainty

The present study considers uncertainties in the bridge's materials, geotechnical parameters, hydrodynamic loads, local scour depths, and sizes of debris accumulation. The variability of the model's input parameters is introduced by multiplying the parameters of the deterministic model by appropriately distributed random variables with a median value of 1.0.

The statistical distributions of the random variables and their correlations are established and computed based on the recommendations found in the literature (Table 3). Most of the random variables are considered uncorrelated, except for the geotechnical character-

istics for which the correlation matrix shown in Table 4 is considered [54]. The concrete elastic modulus is computed according to EN 1992-1-1 [40], and is therefore considered to be fully correlated with the concrete strength. Similarly, the G of the soil is computed considering a fixed Poisson's ratio of 0.3. This results in a full correlation between G and E.

Table 3. Random variables used in the flood vulnerability analysis.

Parameters	Probabilistic Distributions	References
Concrete compressive strength (fcm)	Normal $(\mu = 1, COV = 0.20)$	[55]
Steel yield strength (fsy)	Log − normal $(\widetilde{m} = 1,\ COV = 0.07)$	[56]
Steel elastic modulus (E_s)	Log − normal $(\widetilde{m} = 1,\ COV = 0.03)$	[56]
Soil shear modulus (G)	Log − normal $(\widetilde{m} = 1,\ COV = 0.30)$	[54,57]
Soil effective shear angle (φ')	Normal $(\mu = 1, COV = 0.12)$	[54,57]
Soil unit weight (γ)	Normal $(\mu = 1, COV = 0.10)$	[54]
Hydrodynamic drag forces (F_d)	Normal $(\mu = 1, COV = 0.10)$	[24]
Local scour depth (y_s)	Log − normal $(\widetilde{m} = 0.68,\ COV = 0.16)$	[58]
Debris width (W_d)	Normal $(\mu = 1, COV = 0.10)$	[48]
Debris height (H_d)	Normal $(\mu = 1, COV = 0.25)$	[48]
Debris length (L_d)	Normal $(\mu = 1, COV = 0.25)$	[48]

Table 4. Correlation matrix implemented for the soil characteristics taken from [54].

	G	φ'	γ
G	1.0	0.35	0.45
φ'	0.35	1.0	0.30
γ	0.45	0.30	1.0

2.2.7. Latin Hypercube Sampling

In this study, the Latin Hypercube Sampling (LHS) is operated following [59], whose methodology is well known to be used for uncertainty analysis in seismic engineering (e.g., [60–62]).

The output obtained from the LHS is a set of input model parameters, which defines a set of deterministic numerical models. The set of models is assumed to fully describe the statistical characteristics of the stochastic model. Thus, the propagation of the uncertainty of the model's inputs is achieved by analyzing the models within a set of deterministic numerical analyses. The number of analyses equals the performed number of LHS simulations (N_{sim}). Within each analysis j $(j = \{1 \ldots N_{sim}\})$, a flood analysis is performed to assert whether a designated LS is exceeded or not. For this purpose, an index vector is introduced for each LS and for each pair of $H - v$ values:

$$ind_{LS}\Big(j\ |H, v) = \begin{cases} 0 & if\ LS\ is\ not\ exceed \\ 1 & if\ LS\ is\ exceed \end{cases} \tag{15}$$

The probability of exceeding a designated LS, $P(LS|\ H, v)$, is computed as the ratio between the number of simulations that leads to the exceedance of the designated LS $(N_{LS}(H, v))$ and the total number of simulations N_{sim}:

$$P(LS|\ H, v) = \frac{N_{LS}(H, v)}{N_{sim}} \tag{16}$$

where $N_{LS}(H, v)$ is calculated as the sum of the index vector as follows:

$$N_{LS}(H, v) = \sum_{j=1}^{N_{sim}} ind_{LS}(j \mid H, v) \quad (17)$$

Selecting the optimal number of simulations (N_{sim}) is a fundamental step. The required number of simulations depends on the number of random input variables (N_{var}) and the precision that is aimed to be achieved. Sensitivity analyses can help to obtain the optimal number of simulations for the examined problem. An indication of the required N_{sim} can be found based on the recommendation provided by [60], who suggests that, for practical engineering applications, N_{sim} should be approximately 3timeslarger than the number of input variables (N_{var}). In this study, N_{sim} is set to 40, which is 3.6-times larger than N_{var} ($N_{var} = 11$). The selected N_{sim} produces a tolerance in the estimated LS's probability of 1/40 = 0.025 = 2.5 %, which is considered to be sufficient for practical purposes.

3. Results

3.1. Model Validation

The performance of the proposed model was validated against measured modal periods from a modal survey. The modal survey involved an ambient vibration measurement campaign with 12 tri-axial accelerometers placed on the bridge to measure its response to vibrations from the environment. The results of the measurements were analyzed using operational modal analysis, which allowed the identification of four translational modes of the bridge's deck. However, based on this campaign, it was not possible to obtain the global translational modes of the bridge that would allow for more comprehensive validation of the SSI modelling. An attempt was made to perform a lateral modal analysis with the use of two long-stroke shakers exciting the bridge in the horizontal direction. Unfortunately, this modal survey proved unsuccessful, as it was not possible to excite the bridge sufficiently to obtain a reliable prediction of the bridge's horizontal modes. The validation of the model was thus based on best-available data, although further refinement/calibration could be made if information on horizontal modes would be available.

The comparison of the calculated modal periods with the measured data is presented in Table 5. Results indicated an excellent match between the calculated and measured modal periods from the ambient vibration campaign.

Table 5. Comparison of the calculated and measured modal periods.

No.	Description	Period (s)—Calculated	Period (s)—Measured
1	1st vertical mode of the deck	0.67	0.68
2	Global longitudinal mode	0.58	*ND*
3	2nd vertical mode of the deck	0.41	0.43
4	Global transverse mode	0.36	*ND*
5	Global vertical mode	0.21	*ND*
6	1st transverse mode of the deck	0.21	0.21
7	3rd vertical mode of the deck	0.18	0.19

Comparing mode shapes also indicates good agreement with on-site measurements, though not presented for brevity.

3.2. Vulnerability Analysis

The vulnerability analysis is performed considering both Serviceability and Ultimate limit states for three different scenarios. As an initial scenario, gravity, hydrodynamic, buoyant loading, and local scour are taken into account. As part of the second and third scenarios, debris loading is also included and modelled based on the AS5100.2-2004 standard and Panici and Almeida's model [48], respectively.

3.2.1. Debris Accumulation Sizes

Figure 7 explores the information from Table 2 in more detail. The three panels in Figure 7 display, respectively, the debris accumulation width, height and length as functions of water height for the two different modelling approaches considered herein. With the intention of representing the most significant outcomes, the results obtained with Panici and Almeida's approach [48] are plotted for values of water heights that represent the steady-flow condition and the upper prediction bound. It can be seen that the two modelling approaches diverge the most in the assessment of W_d. Specifically, W_d remains constant with H in the Australian standard, whereas, for Panici and Almeida's approach, W_d decreases and it is also the parameter that is affected the most by the hydraulic conditions. A similar outcome is found for H_d (Figure 7b). However, unlike W_d, H_d increases with the water height when implementing Panici and Almeida's approach. In Figure 7c it is interesting to notice that the implementation of the two different approaches leads to opposite trends in L_d. This is mainly due to the fact that when representing the AS5100.2-2004 guidelines the value of L_d is assumed. Overall, it can be observed that, in steady-flow conditions, Equations (8)–(10) lead to debris accumulations more extended in width and length compared to the ones recommended in the Australian standard. The opposite can be said when considering the case of H_d, where, for higher values of H and v (i.e., upper prediction bound) and most of the H examined, the height of the debris accumulation envisioned in [48] overtakes the one proposed by [36].

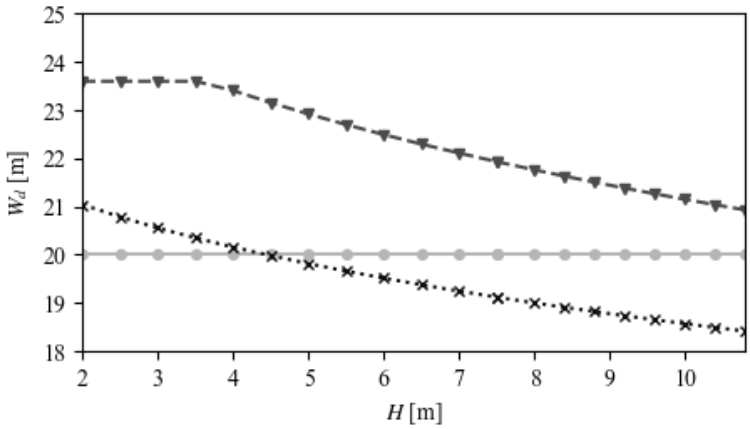

(**a**)

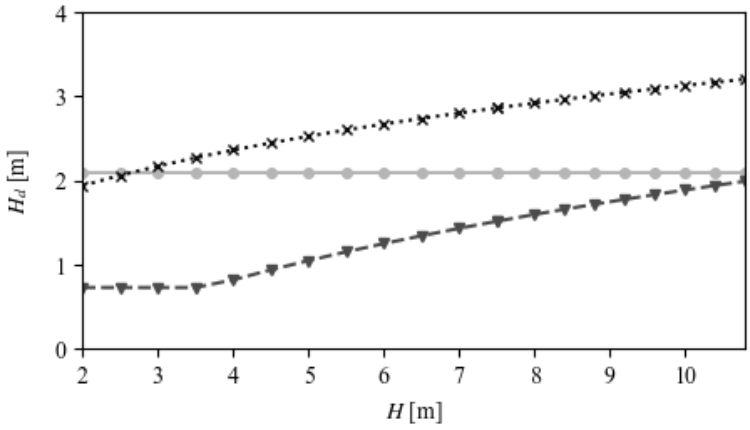

(**b**)

Figure 7. *Cont.*

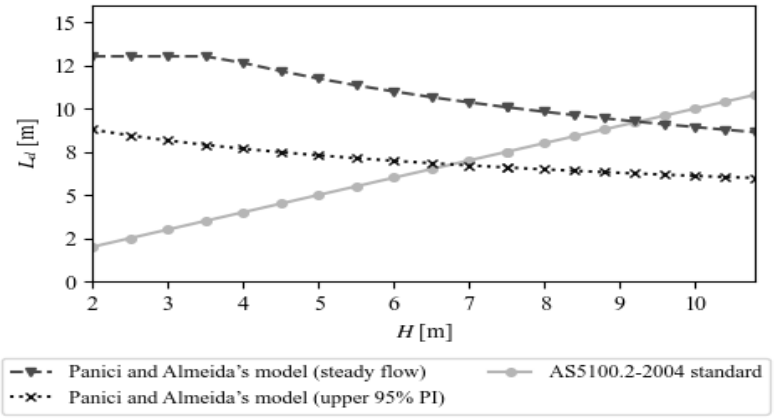

(**c**)

Figure 7. Relationship between (**a**) the width, (**b**) the height, (**c**) the length of debris accumulation and the water height (H) for the two different debris modelling approaches. The results are represented for the steady flow condition and for the upper prediction bound of the regression curve of Figure 3.

3.2.2. Limit State Definition

The conditions for which serviceability and ultimate limit states apply are set based on threshold conditions. The SLS is attained when the percentage of the foundation depth uncovered by the local scour exceeds 50% ($0.5L$ = 2.8 m), or when the water level reaches the top part of the pier (H = 7.5 m). Due to the loading actions and potential accumulation of debris, it is deemed to be too risky to define the SLS at a water height reaching the deck. Hence, to ensure the operability of the bridge, routine inspections are expected to be carried out to monitor the depth of the scour and the water heights. The ULS are met as soon as a single component of the bridge fails. The following failure mechanisms are examined:

- Bending and shear failure at the base of the piers;
- Shear failure of the bearing above the pier and the abutments;
- Bending failure of the deck around the weak axis at the section above the piers and the midspan of the bridge;
- Bearing failure of the foundation (vertical and bending capacity at the base);
- Failure due to local scour reaching the base of the foundation.

The calculation of the ultimate capacity of the structure (ULS) is defined based on the unfactored capacity of the members. The bending capacity of the pier is conservatively defined by the section modulus of the pier and the mean tensile strength of the concrete. Note that the contribution of the reinforcement is neglected, as it is assumed that the amount of reinforcement is below the minimum standard's requirements [40]. The shear strength of the pier is calculated according to equation 6.2a found in [40], which is applicable for members without shear reinforcement. The shear capacities of the shear pin at the middle bearing and the shear keys at the abutment bearing are computed considering the elastic shear resistance indicated in EN-1993-1-1 [39]. The bending capacity of the deck is defined based on the section modulus of the deck in the transverse direction (direction of the flow). The failure of the foundation is assessed with the Meyerhof method [63]. The failure due to local scour is conservatively assumed to be attained when the scour hole reaches the base of the foundation, despite the fact that some capacity is likely to be maintained.

3.2.3. Results for Serviceability Limit State

Figures 8–10 illustrate the vulnerability surfaces obtained for the SLS and the three scenarios (i.e., no debris load, debris load modelled based on AS5100.2-2004, and debris load modelled according to Panici and Almeida's model [48]). As can be seen from figures, the vulnerability surfaces show two distinct regions: one below and one above the pier height (H = 7.5 m). These regions arise as a result of the criteria that have been used for the definition of the SLS. The region below H = 7.5 m represents the SLS of the bridge in

relation to the threshold value set for the scour depths (see Section 3.2.2). On the other hand, the region above H = 7.5 m is the part of the surface for which the SLS of the bridge applies in relation to the threshold value set for the water heights.

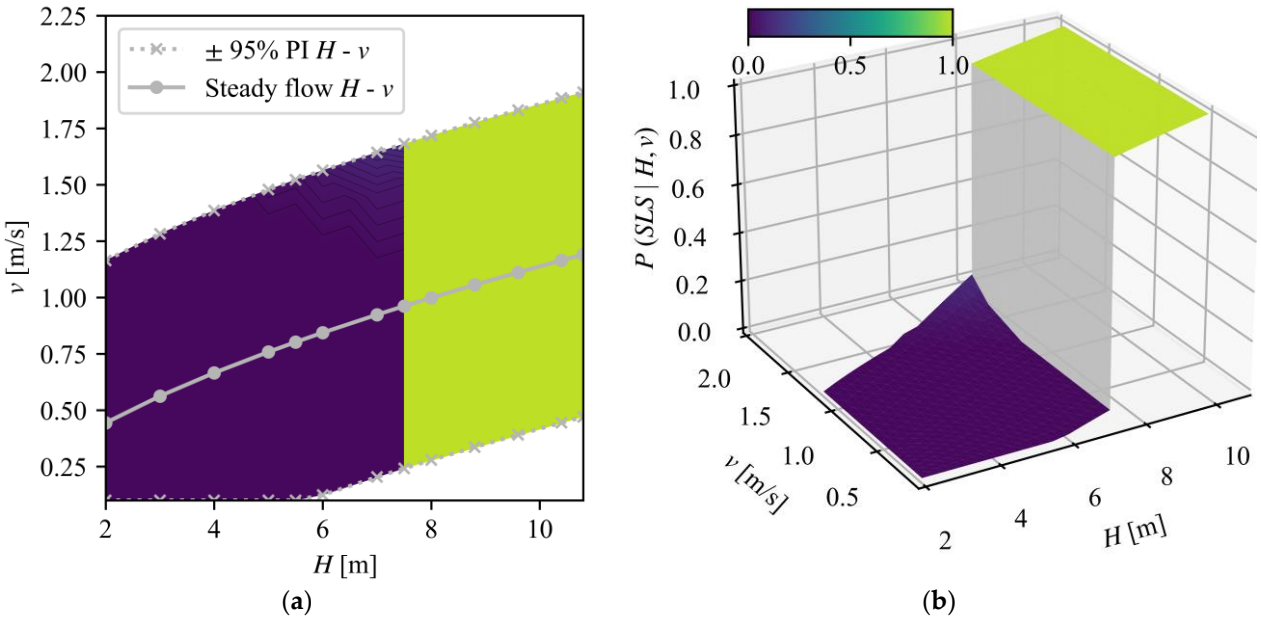

Figure 8. (**a**) Contour and (**b**) 3-D surface plot of the flood vulnerability surface for the serviceability limit state (SLS) for the first scenario (no debris).

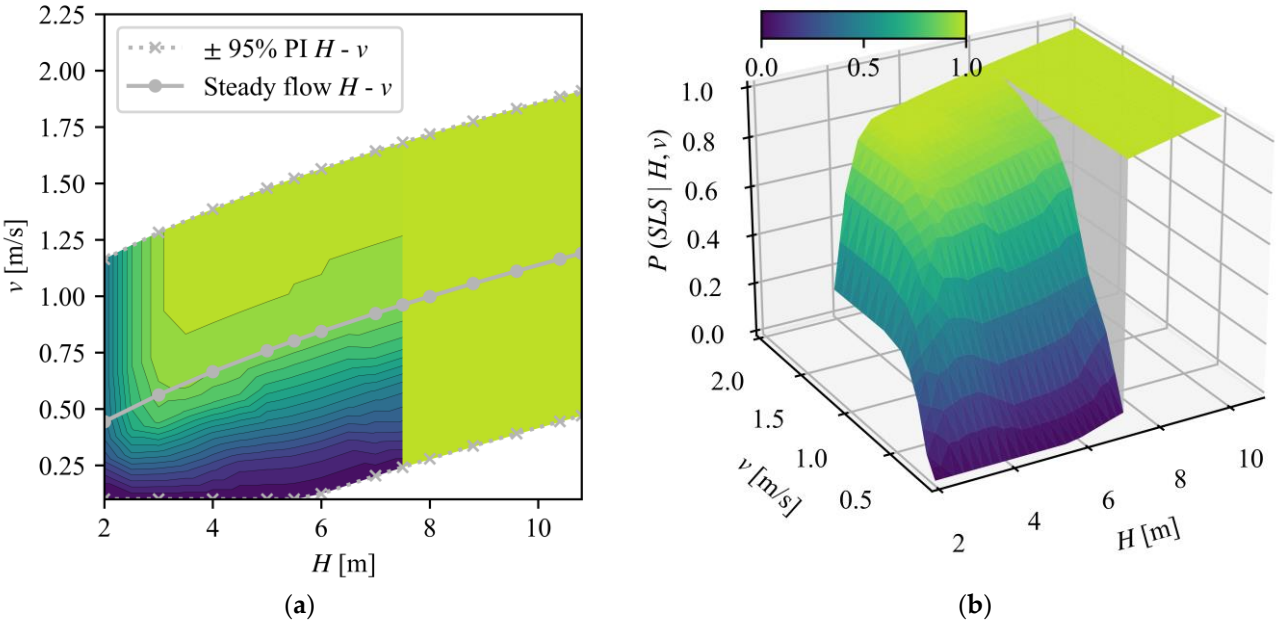

Figure 9. (**a**) Contour and (**b**) 3-D surface plot of the flood fragility surface for the serviceability limit state (SLS) for the second scenario (AS5100.2-2004 standard).

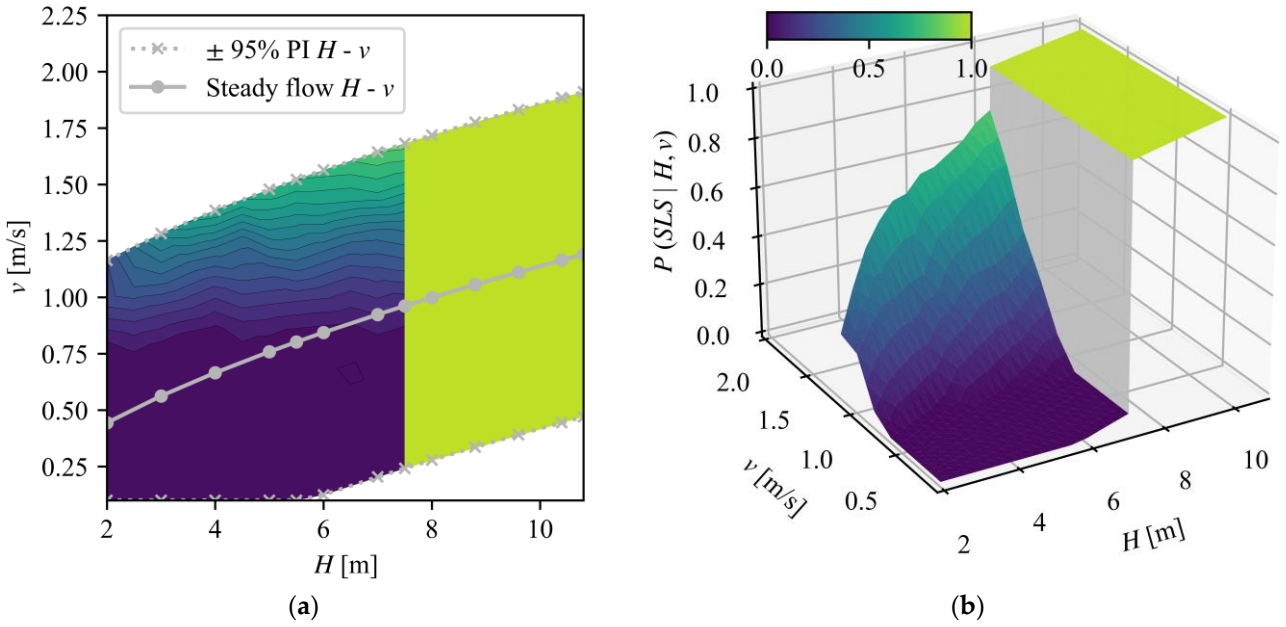

Figure 10. (**a**) Contour and (**b**) 3-D surface plot of the flood fragility surface for the serviceability limit state (SLS) for the third scenario (Panici and Almeida's model [48]).

When comparing Figures 8–10, it is clear that, for high water levels ($H > 7.5$ m), the probability of exceeding the SLS is equal to 1.0 regardless of the scenario considered. On the other hand, for values of $H < 7.5$ m, it is evident that the contributions of the local scour and the mutual interaction between the local scour and debris increase the likelihood of reaching the SLS. In contrast to the first scenario, where local scour has minimal impact on the results, the second scenario has the highest probability of exceeding the SLS. In this case, the SLS is very likely to be exceeded for water heights as low as 3 m (not nearly half of the pier's height) and flow velocities as low as 0.50 m/s. In the third scenario, the vulnerability surface indicates a lower probability of exceeding the SLS compared to the second one and it is mainly occurring in the area located in the upper bound of the $H - v$ relationship. This discrepancy between the results of the second and third scenarios results from the different extent of local scour and, additionally, from adopting different approaches for modelling the shape of the wood accumulation. Indeed, when assessing the vulnerability of the bridge, the shape of the wood accumulation may become more significant than its size. Despite the fact that, for some hydraulic conditions, wood debris sizes may be comparably larger than what is recommended in the AS5100.2-2004 standard (see Figure 7), Panici and Almeida's method [48] provides less unfavorable results. Therefore, it is clear that, in certain circumstances, the bridge is more vulnerable based on the shape of the wood debris loading rather than its size.

3.2.4. Results for Ultimate Limit State

Figures 11–13 represent the vulnerability surfaces obtained for the ULS and the three scenarios. When comparing Figure 11 with Figure 12, and Figure 11 with Figure 13, it is clear that the debris accumulation increases the ULS exceedance probability significantly compared to the scenario without debris. In this latter case, a moderate percentage of failure is expected to occur within the upper bound of the $H - v$ relationship and only for extreme floods (i.e., when the deck is fully submerged) (Figure 11). The use of the standard's modelling approach results in the largest ULS exceedance probabilities (Figure 12), while the results obtained when implementing Panici and Almeida's approach [48] show that the bridge failure is only expected to occur within the upper prediction bound of the $H - v$ relationship (Figure 13).

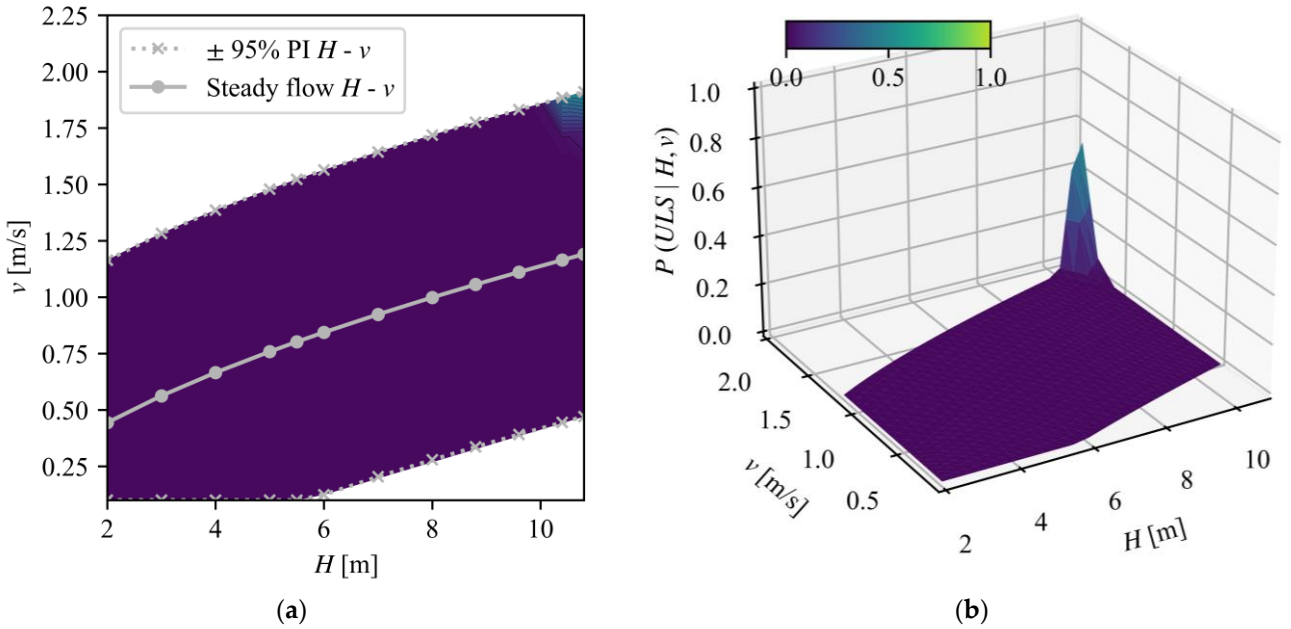

(**a**) (**b**)

Figure 11. (**a**) Contour and (**b**) 3-D surface plot of the flood fragility surface for the ultimate limit state (ULS) for the first scenario (no debris).

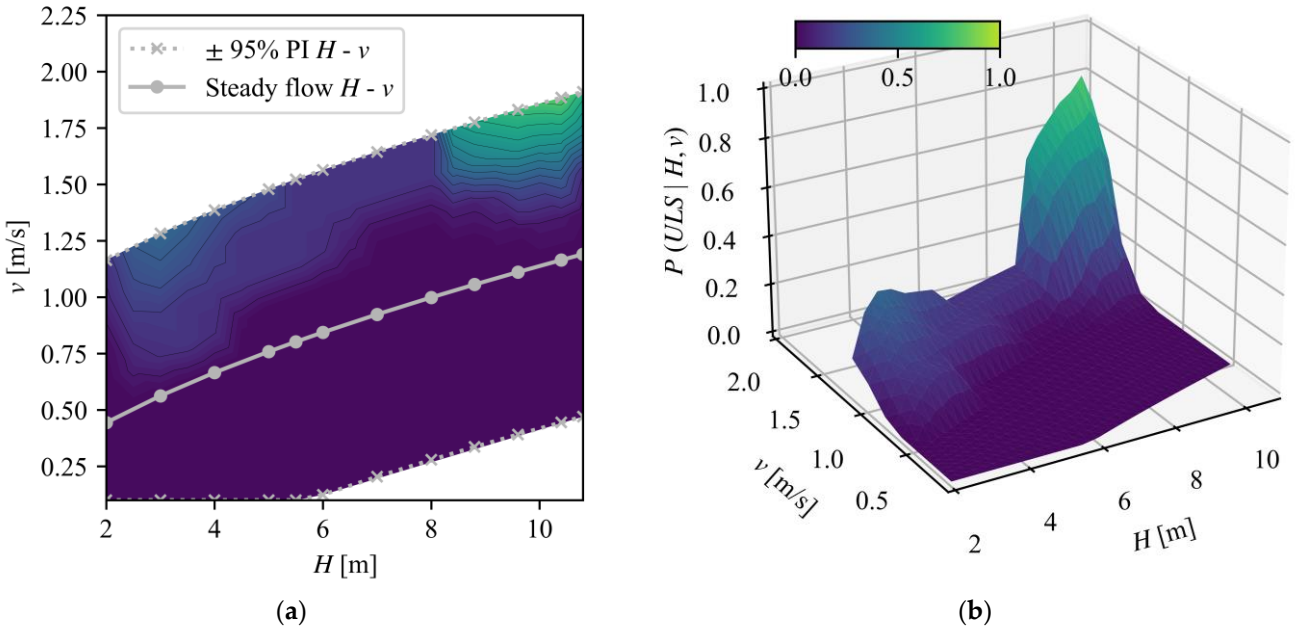

(**a**) (**b**)

Figure 12. (**a**) Contour and (**b**) 3-D surface plot of the flood fragility surface for the ultimate limit state (ULS) for the second scenario (AS5100.2-2004 standard).

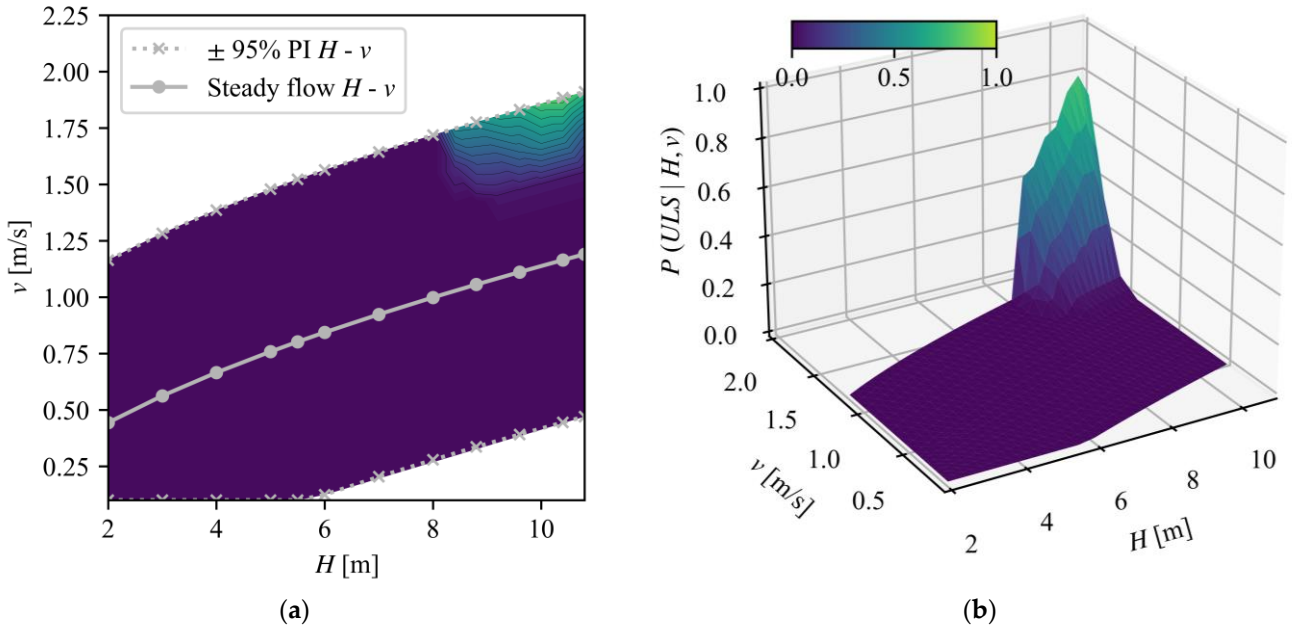

Figure 13. (**a**) Contour and (**b**) 3-D surface plot of the flood fragility surface for the ultimate limit state (ULS) for the third scenario (Panici and Almeida's model [48]).

A detailed examination of Figures 12 and 13 suggests that both debris models yield the largest ULS exceedance probability when the water heights reach the deck (i.e., probability values of approximately 80% for $H > 8.15$). In such a condition, the debris loading is assumed to act over the entire length of the deck, and therefore the hydrodynamic loading on the bridge reaches its maximum value. For water heights lower than the bridge deck, the failure of the bridge appears as an unlikely event when considering the third scenario. On the other hand, for the second scenario, a non-negligible failure probability occurs for water heights approximately equal to 4 m. This is owing to the scour reaching the bottom of the foundation by triggering the failure of the bridge. Such a failure mechanism is not observed when considering the results obtained with Panici and Almeida's model [48], which is found to lead to a less severe scouring compared to the other approach. Hence, even though the area of the debris accumulation in [48] is often bigger, the shape factors from Equations (13) and (14) show that the shape of debris is the leading variable when computing the amplification of local scour. Furthermore, the freedom allowed in the AS5100.2-2004 standard of assigning suggested and custom values to the size and shape of debris accumulations has a relevant role in the overall SLS and ULS exceedance probabilities.

3.3. Sensitivity Analysis

This section examines the extent to which the scour depth is affected by implementing the three scenarios (Section 3.3.1). The bridge's failure utilization ratios are also explored (Section 3.3.2). Note that all the analyses are only implemented for the upper percentile bound (95th percentile) of the $H - v$ relationship, for which the chance of bridge failure is the most pronounced.

3.3.1. Scour Depths

In Figure 14, the 5th, 50th and 95th percentiles of the scour depths are plotted against the water heights for the three scenarios. The values of the scour depths are computed by implementing 40 LHS simulations at each water height, considering the upper bound $H - v$ relationship. The scour depths at which the SLS and ULS are reached are also represented with horizontal dotted lines. As can be noticed, regardless of the percentile examined, the largest scour depths are obtained for the second scenario, whereas the lowest values are attributed to the first scenario. The results obtained with Panici and

Almeida's model [48] mediate the extreme values of scours obtained for the aforementioned cases. When debris accumulation is modelled according to the AS5100.2-2004 standard, the higher amplification of the scour occurs at lower water heights. This phenomenon is less pronounced when implementing the other debris model, for which the amplification of the scour is more uniform over different water heights. As mentioned, this is likely a consequence of a more favorable shape of the debris accumulation (i.e., triangular) that also results in smaller scour depths [56].

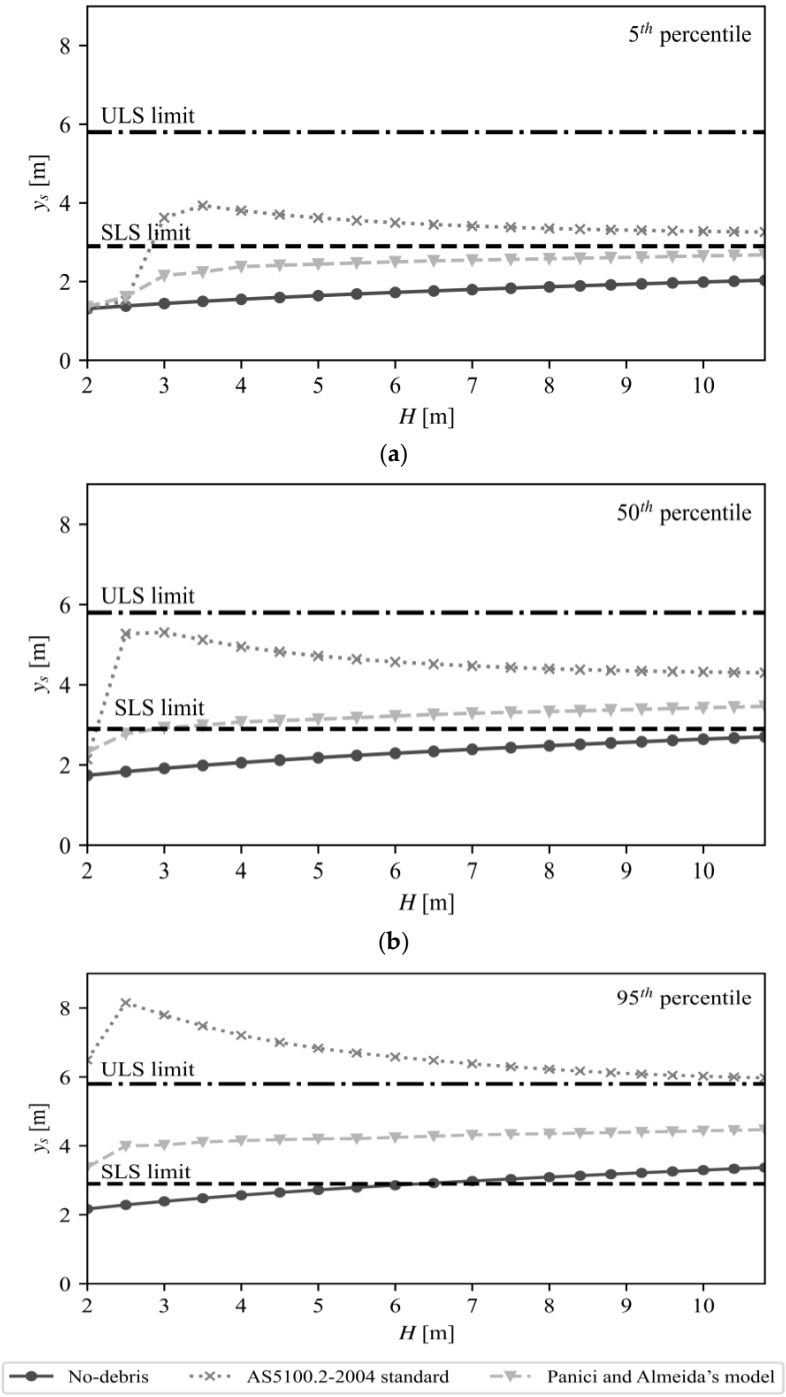

Figure 14. Representation of the (**a**) 5th percentile, (**b**) 50th percentile and (**c**) 95th percentile of scour depths (y_s) against the water heights (H) for the three different scenarios and the upper prediction bound of the $H - v$ relationship.

For the first scenario, the SLS limit state is expected to be exceeded only for a few of the most unfavorable LHS simulations with the largest scour depths (95th percentile). This offers an explanation of the low SLS exceedance probabilities shown in Figure 8 for water height below H = 7.5 m. On the other hand, the high SLS exceedance probability obtained for the second scenario (Figure 9) can be explained by SLS scour depth limit being exceeded even for LHS simulations with the lowest scour predictions (5th percentile). For the third scenario, the high SLS exceedance probabilities occurring for water heights above 3 m (Figure 10) are consistent with the results illustrated in Figure 14b,c, which indicate that the SLS limit is exceeded only for scour depths above the 50th percentile.

By comparing the results in Figure 14, it can be observed that the ULS is only exceeded in the second scenario and the 95th percentile scour-depth prediction (Figure 14c). This tendency supports the non-zero ULS exceedance probabilities shown in Figure 12 for water heights below 8.15 m.

3.3.2. Utilization Ratios for ULS

Figure 15 illustrates the variation of the failure utilization ratio (UR) of the bridge (5th, 50th, and 95th percentiles) against the water heights for the three scenarios and the upper prediction bound of the $H - v$ relationship. The utilization ratio of the bridge is defined as the maximum ratio between the demand and capacity of the individual members of the bridge. A value of utilization ratio larger than 1 indicates the failure of the bridge (exceedance of the ULS as defined in Section 3.2.2). The 5th, 50th and 95th percentiles utilization ratios of the bridge are obtained by performing 40 LHS simulations for each water height and related upper-bound velocity. In the scenario with no debris, the exceedance of the ULS of the bridge is only expected to occur for water heights above 10 m and for a value of utilization ratio above the 50th percentile. This condition results in a failure probability equal to roughly 50%, which is consistent with the results in Figure 11. In the case when debris accumulation is modelled according to AS5100.2-2004 standard, the exceedance of the ULS is expected over the entire range of water heights for the 95% percentile of utilization ratio, reaching particularly high values when the water height reaches the deck (H > 8.15 m). This outcome is in line with what is shown in Figure 12, in which the non-zero ULS exceedance probabilities are reached over the entire upper part of the vulnerability surface.

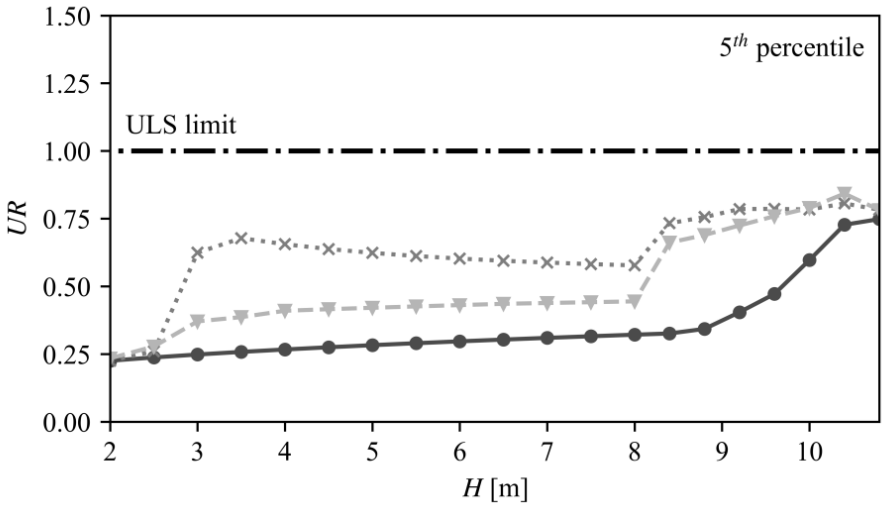

(**a**)

Figure 15. *Cont.*

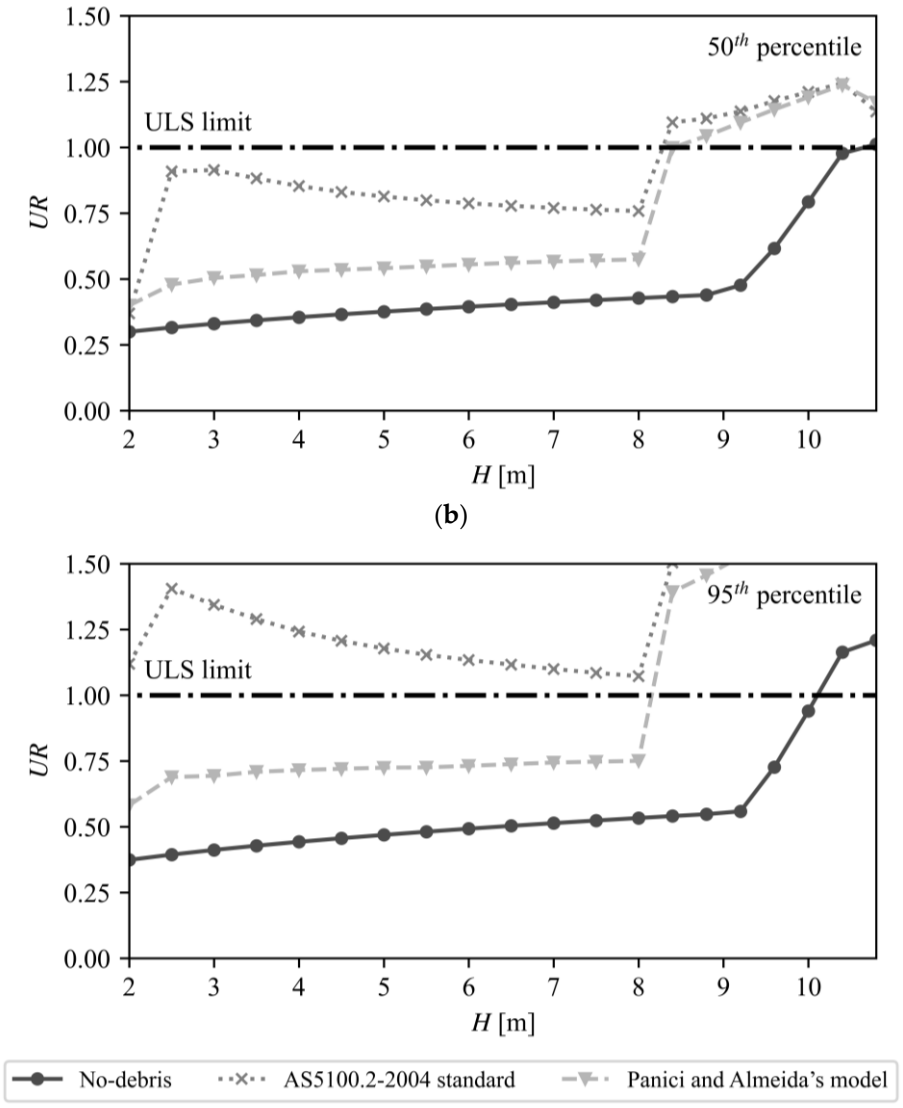

Figure 15. Representation of the (**a**) 5th, (**b**) 50th, and (**c**) 95th percentiles of the failure utilization ratios (UR) against the water heights (H) for the three different scenarios and for the upper prediction bound of the $H - v$ relationship.

On the other hand, when modelling the debris loading with Panici and Almeida's model [48], the 50th and 95th percentiles of utilization ratios exceed the ULS limit only for water heights above 8.15 m, thus explaining the results from Figure 13.

Assessing the maximum values of UR across the ULS simulations enables the identification of the leading mechanism that threatens the bridge's performance (i.e., the mechanism with the largest UR). In this context, the most critical mechanisms are identified as the local scour and the failure of the pier-bearing system. Figure 16 displays the frequency of occurrence of such mechanisms within 40 LHS simulations for the different scenarios and within the upper prediction bound of the $H - v$ relationship. Overall, regardless of the scenario considered, the local scour proves to be the predominant mechanism (i.e., with maximum utilization ratio) within a range of water height between 2 and 8.15 m. When the water reaches the bridge deck, the loss of the bridge's performance is predominantly associated with a compromised functionality of the pier-bearing system. The results, however, differ depending on the scenario considered. Data reveal that when wood debris forces are neglected, the potential of the deck unseating due to the failure of the pier bearing

(Figure 16a) is less pronounced compared to Figure 16b,c, in which a higher frequency of bearing failure is obtained at lower water height. At the same time, it is clear that the implementation of two different wood debris models has a minor impact on the frequency of occurrence of both mechanisms.

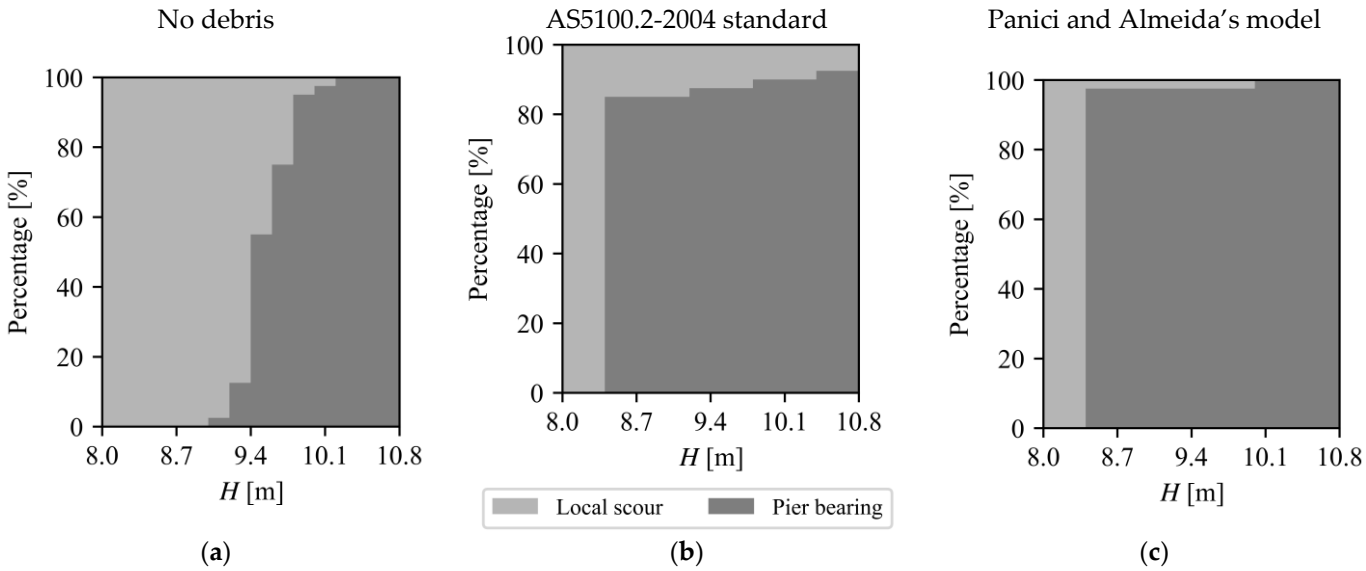

Figure 16. Frequency of occurrence of two leading mechanisms (i.e., local scour and pier bearing failure) within LHS simulations for the (**a**) first, (**b**) second, and (**c**) third debris scenario and the upper prediction bound of the $H - v$ relationship. Note that the frequencies between H = 2 m and H = 8 m are omitted, since, in this range, local scour is the leading mechanism.

4. Discussion

In this paper, a flood vulnerability analysis of a real-case roadway bridge is performed. The vulnerability of the bridge is examined by considering the concurrent action of gravity loads, hydrodynamic loads, wood debris accumulation and local scour. The interaction between local scour and the accumulation of debris is also considered, and its implementation is based on an equivalent-pier-width approach. Due to the lack of stationary hydraulic conditions at the site, the vulnerability analysis is performed with consideration of both flow velocity and water height as input parameters. This leads to the representation of the vulnerability analysis results as a surface in a three-dimensional domain.

The main purpose of this paper is to examine the results of three different scenarios. One examines the condition with no debris, while the second and third evaluate two different debris modelling approaches. The first approach relies on the recommendations drawn from the AS5100.2-2004 standard, whereas the second approach refers to the model proposed by Panici and Almeida [48], which, compared to the standards-based methodology, involves a more elaborate and refined analytical procedure. The research of the second approach is motivated by the absence of accurate guidelines for modelling processes of wood debris accumulation at bridge piers.

Based on the results, it is clear that the bridge is more likely to exceed its serviceability and ultimate limit states in presence of wood debris compared to the condition with no debris. The accumulation of debris at the bridge pier is shown to be responsible for the increase in local scour depths. As the debris and scour action interact, the SLS and ULS of the bridge occur for smaller flooding events compared to the scenario with no debris. Nevertheless, the bridge is more likely to fail for values of H and v located in the upper prediction interval of the $H - v$ relationship. This finding is not dependent on the modelling approach considered. Overall, the results of this study indicate that the use of Panici and Almeida's model [48] offers less conservative estimates of the bridge response to severe floodings. This may be due to the fact that the novel modelling approach is able to provide

a more analytical definition of the size and shape of the debris accumulation. The triangular shape, in fact, yields less severe scouring depths compared to the use of the rectangular shape suggested in the AS5100.2-2004 standard [53].

A sensitivity analysis is also performed and is used to examine the variation of the scour depths, bridge's utilization ratios and governing failure mechanisms for the three scenarios and different water heights. From this analysis, it is shown that the AS5100.2-2004 standard produces the most unfavorable results. For instance, the exceedance of the ultimate limit states due to scour only occurs when implementing the recommendations provided in the Australian Standard. A similar outcome occurs when examining the values of utilization ratios of the structure. It is clear that for most of the values of H, the AS5100.2-2004 Standard is the only scenario that leads to the exceedance of the ULS for the highest values of the utilization ratio (95% percentile). It also emerges that local scour plays a crucial role in most of the hydraulic conditions considered, and its influence is more significant for the second scenario than the third. This confirms what was found in the literature [64] and makes it clear that computing the magnitude of the local scour is essential when examining bridge vulnerability to flood and bridge failure modes. For water height reaching the deck, the performance of the bridge is mainly threatened by the failure of the pier bearing instead. However, in this case, the difference between the two debris models becomes less evident.

In spite of the effectiveness of the presented vulnerability approach, there are limitations that need to be taken into account. For instance, the poor quality and amount of hydraulic data and a lack of an appropriate numerical modelling approach do not allow a reasonable estimation of the hydrodynamic-related loads. Hydraulic data input are essential in flood vulnerability analysis. Hence, more appropriate and consistent monitoring of the hydraulic variables is encouraged as it can be extremely beneficial in the vulnerability assessment of riverine bridges. Similarly, the knowledge gap related to the mechanisms governing the accumulation of debris jams at bridge piers, as well as the lack of monitoring data on wood debris recruitment and transportation represents a limitation for the reliability of the results of the analysis. Another aspect to consider is the simplified finite-element modelling employed in this study, which, due to a complicated interaction between the structure, soil, hydrodynamic loads and local scour, owns further examinations. A similar evaluation applies to the coefficient of variations of the materials, geotechnical characteristics, hydrodynamic forces, local scour depth and size of wood debris accumulation. The values assigned to the coefficient of variations are, in fact, based on isolated recommendations found in the literature. Moreover, important processes such as *afflux,* river bed-load transport and the degradation of the bridge's materials are not included in the analysis as the present study does not account for the time-dependent assessment of the bridge's vulnerability. Due to the complex interplay between debris loads, scour, and hydraulic forces, the research examination assessing bridge flood vulnerability should be carefully addressed. Despite the acknowledged limitations, the presented framework bridges some of the gaps existing in the standards-based approach providing a more up-to-date and faithful methodology for bridge vulnerability analysis. Therefore, more effort should be devoted to improving and updating the existing standards and guidelines concerning the modelling of hydrodynamic-related processes. Particularly, the interplay between debris accumulation and local scour would need further examination as it is shown to substantially affect the bridge's vulnerability.

It is hoped that this study will inspire future research into improving and upgrading the vulnerability analysis framework. For instance, the implementation of faithful hydraulic numerical modelling techniques, along with local scour monitoring solutions, can help to validate the proposed modelling approach and assess the performance of the asset throughout its lifespan. At the same time, the developed approach represents a valuable tool for supporting targeted visual inspection and Structural Health Monitoring campaigns. Vulnerability surfaces can provide useful insight into the selection of the key parameters that should be verified and monitored at different stages of a bridge's life-cycle

to determine its level of performance [65]. Furthermore, considering a life-cycle perspective, bridge vulnerability assessment is also beneficial for quantitatively determining the risk severity of hazards on bridges and helping to evaluate the effectiveness of potential resilient countermeasures for risk mitigation. This study can provide policymakers, engineering consultants, bridge engineers and stakeholders with a valid and reliable method of estimating the anticipated economic and functional losses associated with flooding hazards, implementing effective decision-making processes, and selecting sustainable and resilient strategies.

Author Contributions: Conceptualization, methodology M.K., A.A. and V.B.; software, validation, formal analysis, M.K.; investigation, resources, data curation M.K., A.A. and V.B.; writing—original draft preparation, M.K.; writing—review and editing, A.A. and V.B.; visualization, M.K. and A.A. and V.B.; project administration, A.A.; funding acquisition, A.A. All authors have read and agreed to the published version of the manuscript.

Funding: This research was funded by the European Union Civil Protection Mechanism, under the UCPM-2019-PP-AG call, Grant Agreement Number 874421, oVERFLOw project (Vulnerability assessment of embankments and bridges exposed to flooding hazard). The authors would also like to express their gratitude for the support received from the Slovenian Research Agency: research core funding No. P2-0273 and from the infrastructure program: No. I0-032.

Institutional Review Board Statement: Not applicable.

Informed Consent Statement: Not applicable.

Data Availability Statement: Not applicable.

Conflicts of Interest: The authors declare no conflict of interest.

List of Symbols and Notations

a	Pier width
a_d^*	Equivalent pier width
A_d	Projected wetted area in the direction of the flow
A_l	Wetted area perpendicular to the flow
c'	Effective cohesion of the soil
C_d	Drag coefficient
C_l	Lift coefficient
CPT	Cone Penetration Test
D	Diameter of a well foundation
D_E	Embedment depth of the foundation
D_L	Length of the deck
d_{sp}	Wetted depth of the deck
d_{ss}	Wetted depth of the solid superstructure
d_{wgs}	Distance from the girder soffit to the flood water surface
E	Soil elastic modulus
E_s	Steel elastic modulus
f_{cm}	Concrete compressive strength
f_{sy}	Steel yield strength
F_d	Hydrodynamic drag force
F_l	Hydrodynamic lift force
F_{rL}	Debris Froude number
F_r	Froude number
g	Gravitational acceleration
G	Shear modulus of the soil
H	Water height
H_d	Height of wood debris accumulation
IM	Intensity measure

$ind_{LS}(j\|H,v)$	Index vector for each LS and each *H-v*
j	Index of *j*-th LHS simulation
K_1	Correction factor for the pier nose shape
K_2	Correction factor for the angle of attack flow
K_3	Correction factor for the riverbed condition
$K_{d,1}K_{d,2}$	Correction factors used in the calculation of the equivalent pier width depending on the shape of the debris raft
K_H^e	Horizontal embedded stiffness of the well foundation
K_R^e	Rocking embedded stiffness of the well foundation
K_V^e	Vertical embedded stiffness of the well foundation
K_T^e	Torsional embedded stiffness of the well foundation
L	Depth of the foundation
L_d	Length of wood debris accumulation in the flow direction
L_L	Key log length
LHS	Latin Hypercube Sampling
LS	Limit state
N_{60}	Equivalent number of Standard Penetration Test (SPT) blows of the soil
$N_{LS}(H,v)$	Number of simulations that leads to the exceedance of LS for a given *H-v*
N_{sim}	Number of LHS simulations
N_{var}	Number of random input variables
$P(LS\|H,v)$	Probability of exceeding the designated LS for a given *H-v*
PI	Prediction Intervals
P_r	Proximity ratio
Q	Water discharge
RC	Reinforced Concrete
R_f	Foundation radius
S_L	Span length of the bridge
S_r	Relative submergence of the deck
SLS	Serviceability Limit State
SSI	Soil–Structure Interaction
ULS	Ultimate Limit State
UR	Utilization ratio
v	Mean flow velocity
W_d	Width of wood debris accumulation
y_{gs}	Average vertical distance from the girder soffit to the riverbed
y_s	Local scour depth
φ'	Effective shear angle of the soil
γ	Soil unit weight
ν	Poisson's ratio
θ	Angle of flow attack

References

1. Jean-Louis, J.B.; Paolo, G.; Congpu, Y. Statistical, Risk, and Reliability Analyses of Bridge Scour. *J. Geotech. Geoenviron. Eng.* **2014**, *140*, 4013011. [CrossRef]
2. Benn, J. Railway bridge failure during flooding in the UK and Ireland. *Proc. Inst. Civ. Eng. Forensic Eng.* **2013**, *166*, 163–170. [CrossRef]
3. Kumalasari, W.; Hadipriono, F.C. Analysis of Recent Bridge Failures in the United States. *J. Perform. Constr. Facil.* **2003**, *17*, 144–150. [CrossRef]
4. Zampieri, P.; Zanini, M.A.; Faleschini, F.; Hofer, L.; Pellegrino, C. Failure analysis of masonry arch bridges subject to local pier scour. *Eng. Fail. Anal.* **2017**, *79*, 371–384. [CrossRef]
5. Stefanidis, S.; Alexandridis, V.; Theodoridou, T. Flood exposure of residential areas and infrastructure in Greece. *Hydrology* **2022**, *9*, 145. [CrossRef]
6. Karatzetzou, A.; Stefanidis, S.; Stefanidou, S.; Tsinidis, G.; Pitilakis, D. Unified hazard models for risk assessment of transportation networks in a multi-hazard environment. *Int. J. Disaster Risk Reduct.* **2022**, *75*, 102960. [CrossRef]
7. Banerjee, S.; Shinozuka, M. Nonlinear Static Procedure for Seismic Vulnerability Assessment of Bridges. *Comput. Civ. Infrastruct. Eng.* **2007**, *22*, 293–305. [CrossRef]
8. Ma, X.; Zhang, W. Dynamic amplification responses of short span bridges considering scour and debris impacts. *Eng. Struct.* **2022**, *252*, 113644. [CrossRef]

9. Pagliara, S.; Carnacina, I. Influence of wood debris accumulation on bridge pier scour. *J. Hydraul. Eng.* **2011**, *137*, 254–261. [CrossRef]
10. Prendergast, L.J.; Gavin, K. A review of bridge scour monitoring techniques. *J. Rock Mech. Geotech. Eng.* **2014**, *6*, 138–149. [CrossRef]
11. Ebrahimi, M.; Djordjević, S.; Panici, D.; Tabor, G.; Kripakaran, P. A method for evaluating local scour depth at bridge piers due to debris accumulation. In Proceedings of the Institution of Civil Engineers—Bridge Engineering; Thomas Telford Ltd.: London, UK, 2020; Volume 173, pp. 86–99.
12. Shen, H.W.; Schneider, V.R.; Karaki, S. Local scour around bridge piers. *J. Hydraul. Div.* **1969**, *95*, 1919–1940. [CrossRef]
13. Lagasse, P.F. *Countermeasures to Protect Bridge Piers from Scour*; Transportation Research Board: Washington, DC, USA, 2007; Volume 593.
14. Lin, C.; Han, J.; Bennett, C.; Parsons, R.L. Case history analysis of bridge failures due to scour. In *Climatic Effects on Pavement and Geotechnical Infrastructure*; American Society of Civil Engineers: Reston, VA, USA, 2014; pp. 204–216.
15. Zhang, Y. Economic Impact of Bridge Damage in a Flood Event. Master's Thesis, RMIT University, Melbourne, Australia, 2016.
16. Stewart, M.G. Reliability-based assessment of ageing bridges using risk ranking and life cycle cost decision analyses. *Reliab. Eng. Syst. Saf.* **2001**, *74*, 263–273. [CrossRef]
17. Billah, A.; Alam, M.S. Seismic fragility assessment of highway bridges: A state-ofthe-art review. *Struct. Infrastruct. Eng.* **2015**, *11*, 804–832. [CrossRef]
18. Karamlou, A.; Bocchini, P. Computation of bridge seismic fragility by large-scale simulation for probabilistic resilience analysis. *Earthq. Eng. Struct. Dyn.* **2015**, *44*, 1959–1978. [CrossRef]
19. Mosleh, A.; Jara, J.; Razzaghi, M.S.; Varum, H. Probabilistic seismic performance analysis of RC bridges. *J. Earthq. Eng.* **2020**, *24*, 1704–1728. [CrossRef]
20. Turmo, J.; Ramos, G.; Aparicio, A.C. Shear truss analogy for concrete members of solid and hollow circular cross section. *Eng. Struct.* **2009**, *31*, 455–465. Available online: http://www.sciencedirect.com/science/article/B6V2Y-4TMYJYT-1/2/8f69b9f83b0bb052df05ff98d8a38d13 (accessed on 20 December 2022). [CrossRef]
21. Kappos, A.J.; Saiid, S.M.; Nuray, A.M.; Isaković, I. (Eds.) *Seismic Design and Assessment of Bridges*; Spinger: Berlin/Heidelberg, Germany, 2012.
22. Deco, A.; Frangopol, D.M. Risk assessment of highway bridges under multiple hazards. *J. Risk Res.* **2011**, *14*, 1057–1089. [CrossRef]
23. Dong, Y.; Frangopol, D.M.; Saydam, D. Time-variant sustainability assessment of seismically vulnerable bridges subjected to multiple hazards. *Earthq. Eng. Struct. Dyn.* **2013**, *42*, 1451–1467. [CrossRef]
24. Kim, H.; Sim, S.-H.; Lee, J.; Lee, Y.-J.; Kim, J.-M. Flood fragility analysis for bridges with multiple failure modes. *Adv. Mech. Eng.* **2017**, *9*, 1687814017696415. [CrossRef]
25. Ahamed, T.; Duan, J.G.; Jo, H. Flood-fragility analysis of instream bridges—Consideration of flow hydraulics, geotechnical uncertainties, and variable scour depth. *Struct. Infrastruct. Eng.* **2021**, *17*, 1494–1507. [CrossRef]
26. Argyroudis, S.A.; Mitoulis, S.A. Vulnerability of bridges to individual and multiple hazards—Floods and earthquakes. *Reliab. Eng. Syst. Saf.* **2021**, *210*, 107564. [CrossRef]
27. Tanasić, N.; Ilić, V.; Hajdin, R. Vulnerability assessment of bridges exposed to scour. *Transp. Res. Rec.* **2013**, *2360*, 36–44. [CrossRef]
28. Anisha, A.; Jacob, A.; Davis, R.; Mangalathu, S. Fragility functions for highway RC bridge under various flood scenarios. *Eng. Struct.* **2022**, *260*, 114244. [CrossRef]
29. George, J.; Menon, A. Analytical fragility curves for displacement-based scour assessment of masonry arch bridges. In *Structures*; Elsevier: Amsterdam, The Netherlands, 2022; Volume 46, pp. 172–185.
30. Homaei, F.; Najafzadeh, M. Failure analysis of scouring at pile groups exposed to steady-state flow: On the assessment of reliability-based probabilistic methodology. *Ocean Eng.* **2022**, *266*, 112707. [CrossRef]
31. Homaei, F.; Najafzadeh, M. A reliability-based probabilistic evaluation of the wave-induced scour depth around marine structure piles. *Ocean Eng.* **2020**, *196*, 106818. [CrossRef]
32. Kwon, O.-S.; Elnashai, A. The effect of material and ground motion uncertainty on the seismic vulnerability curves of RC structure. *Eng. Struct.* **2006**, *28*, 289–303. [CrossRef]
33. Bartlett, F.M.; MacGregor, J.G. Statistical analysis of the compressive strength of concrete in structures. *Mater. J.* **1996**, *93*, 158–168.
34. Kolisko, J.; Hunka, P.; Jung, K. A statistical analysis of the modulus of elasticity and compressive strength of concrete C45/55 for pre-stressed precast beams. *J. Civ. Eng. Archit.* **2012**, *6*, 1571.
35. Yáñez-Godoy, H.; Mokeddem, A.; Elachachi, S.M. Influence of spatial variability of soil friction angle on sheet pile walls' structural behaviour. *Georisk Assess. Manag. Risk Eng. Syst. Geohazards* **2017**, *11*, 299–314. [CrossRef]
36. Breysse, D.; Niandou, H.; Elachachi, S.; Houy, L. A generic approach to soil–structure interaction considering the effects of soil heterogeneity. *Geotechnique* **2005**, *55*, 143–150. [CrossRef]
37. Tubaldi, E.; White, C.J.; Patelli, E.; Mitoulis, S.A.; de Almeida, G.; Brown, J.; Cranston, M.; Hardman, M.; Koursari, E.; Lamb, R.; et al. Invited perspectives: Challenges and future directions in improving bridge flood resilience. *Nat. Hazards Earth Syst. Sci.* **2021**, *22*, 795–812. [CrossRef]
38. Diehl, T.H. *Potential Drift Accumulation at Bridges*; US Department of Transportation, Federal Highway Administration, Research and Development, Turner-Fairbank Highway Research Center: McLean, VA, USA, 1997.

39. *European Standard EN 1993-1-1:2005*; Eurocode 3: Design of Steel Structures—Part 1-1: General Rules and Rules for Buildings. European Committee for Standardization (CEN): Brussels, Switzerland, 2005.
40. *European standard EN 1992-1-1:2004*; Eurocode 2: Design of Concrete Structures—Part 1-1: General Rules and Rules for Buildings. European Committee for Standardization (CEN): Brussels, Switzerland, 2004.
41. Herschy, R.W. *Streamflow Measurement*; CRC Press: Boca Raton, FL, USA, 2008.
42. Zhu, M. *The OpenSeesPy Library*, Version 3.2.2—2020. 2020. Available online: https://openseespydoc.readthedocs.io/en/latest/ (accessed on 1 November 2022).
43. McKenna, F.; Fenves, G.L.; Scott, M.H. *Open System for Earthquake Engineering Simulation (OpenSees)*; Pacific Earthquake Engineering Research Center, University of California: Berkeley, CA, USA, 2020.
44. Pais, A.; Kausel, E. Approximate formulas for dynamic stiffnesses of rigid foundations. *Soil Dyn. Earthq. Eng.* **1988**, *7*, 213–227. [CrossRef]
45. *Australian Standard AS-5100.2-2004*; Bridge Desing—Part 2: Design Loads. Standards Australia: Sydney, Australia, 2004.
46. Yung-Yen, K.; Jiunn-Shyang, C.; Yu-Ching, T.; Cheng-Hsing, C.; Helsin, W.; Chung-Yue, W. Evaluation of Flood-Resistant Capacity of Scoured Bridges. *J. Perform. Constr. Facil.* **2014**, *28*, 61–75. [CrossRef]
47. Hung, C.-C.; Yau, W.-G. Vulnerability evaluation of scoured bridges under floods. *Eng. Struct.* **2017**, *132*, 288–299. [CrossRef]
48. Panici, D.; de Almeida, G.A.M. Formation, growth, and failure of debris jams at bridge piers. *Water Resour. Res.* **2018**, *54*, 6226–6241. [CrossRef]
49. Hess, J.M. *Distribution and Residence Times of Large Woody Debris along South River, Shenandoah Valley, Virginia*; University of Delaware: Newark, DE, USA, 2007.
50. Gurnell, A.; Bertoldi, W. Wood in fluvial systems. In *Treatise on Geomorphology*; Elsevier: Amsterdam, The Netherlands, 2020.
51. Schwarz, U. Sava white book. In *River Sava: Threats and Restoration Potential*; EuroNatur/Riverwatch: Radolfzell/Wien, Germany/Austria, 2016.
52. Arneson, L.A.; Zevenbergen, L.W.; Lagasse, P.F.; Clopper, P.E. *Evaluating Scour at Bridges. HEC-18*, 5th ed.; Hydraulic Engineering Circular No. 18.; National Highway Institute: Wahington, DC, USA, 2012.
53. Lagasse, P.F.; Zevenbergen, L.W.; Clopper, P.E. Effects of debris on bridge pier scour. In Proceedings of the 5th International Conference on Scour and Erosion (ICSE-5), San Francisco, CA, USA, 7–11 November 2010; pp. 854–863.
54. Zhang, Y. Probabilistic Structural Seismic Performance Assessment Methodology and Application to an Actual Bridge-Foundation-Ground System. Ph. D. Thesis, University of California, San Diego, CA, USA, 2006.
55. Melchers, R.E. *Structural Reliability Analysis and Prediction*; Wiley: Hoboken, NJ, USA, 1999.
56. JCSS. *Probabilistic Model Code*; Part 3, Resistance models, Section 3.0, Static Properties of Structural Steel; JCSS: 2001. Available online: https://www.jcss-lc.org/publications/jcsspmc/part_iii.pdf (accessed on 5 December 2022).
57. Aygün, B.; Dueñas-Osorio, L.; Padgett, J.E.; DesRoches, R. Efficient Longitudinal Seismic Fragility Assessment of a Multispan Continuous Steel Bridge on Liquefiable Soils. *J. Bridg. Eng.* **2011**, *16*, 93–107. [CrossRef]
58. Johnson, P.A.; Clopper, P.; Zevenbergen, L.; Lagasse, P.F. Quantifying Uncertainty and Reliability in Bridge Scour Estimations. *J. Hydraul. Eng.* **2015**, *141*. [CrossRef]
59. Vořechovský, M.; Novák, D. Correlation control in small-sample Monte Carlo type simulations I: A simulated annealing approach. *Probabilistic Eng. Mech.* **2009**, *24*, 452–462. [CrossRef]
60. Dolsek, M. Incremental dynamic analysis with consideration of modeling uncertainties. *Earthq. Eng. Struct. Dyn.* **2009**, *38*, 805–825. [CrossRef]
61. Dolšek, M. Simplified method for seismic risk assessment of buildings with consideration of aleatory and epistemic uncertainty. *Struct. Infrastruct. Eng.* **2012**, *8*, 939–953. [CrossRef]
62. Kosič, M.; Dolšek, M.; Fajfar, P. Dispersions for the pushover-based risk assessment of reinforced concrete frames and cantilever walls. *Earthq. Eng. Struct. Dyn.* **2016**, *45*, 2163–2183. [CrossRef]
63. Meyerhof, G.G. Some Recent Research on the Bearing Capacity of Foundations. *Can. Geotech. J.* **1963**, *1*, 16–26. [CrossRef]
64. Ligthart, F. *Failure Mechanisms of Bridge Structures under Natural Hazards*; RMIT University: Melbourne, Australia, 2015.
65. Tanasic, N.; Hajdin, R. Performance indicators for bridges exposed to a flooding hazard. In Proceedings of the Joint COST TU 1402—COST TU 1406-IABSE WC1 Workshop, Zagreb, Croatia, 2–3 March 2017.